Seasonal and interannual variation of equatorial waves in ERA5 and GloSea5

Yang, G.-Y. ORCID: https://orcid.org/0000-0001-7450-3477, Feng, X. ORCID: https://orcid.org/0000-0003-4143-107X and Hodges, K. ORCID: https://orcid.org/0000-0003-0894-229X
(2023) Seasonal and interannual variation of equatorial waves in ERA5 and GloSea5. Quarterly Journal of the Royal Meteorological Society, 149 (752). pp. 1109-1134. ISSN 1477-870X doi: 10.1002/QJ.4460 Available at https://centaur.reading.ac.uk/111433/

Received: 18 January 2023 | Revised: 21 March 2023 | Accepted: 23 March 2023

DOI: 10.1002/qj.4460

Quarterly Journal of the Royal Meteorological Society RMetS

RESEARCH ARTICLE

Seasonal and interannual variation of equatorial waves in ERA5 and GloSea5

Gui-Ying Yang | **Xiangbo Feng** | **Kevin Hodges**

National Centre for Atmospheric Science, Department of Meteorology, University of Reading, Reading, UK

Correspondence
Gui-Ying Yang, National Centre for Atmospheric Science, Department of Meteorology, University of Reading, Earley Gate, Reading RG6 6ET, UK.
Email: g.y.yang@reading.ac.uk

Funding information
the Weather and Climate Science for Services Partnership (WCSSP) Southeast Asia; The National Centre for Atmospheric Science through the NERC National Capability Internaltional Programmes, Grant/Award Number: NE/X006263/1

Abstract

This study presents an analysis of the equatorial waves in the ERA5 reanalysis and forecasts of the Met Office Global Seasonal Forecast System version 5 (GloSea5), by projecting dynamical fields onto theoretical equatorial wave modes. The seasonal and interannual variation of equatorial wave activity in GloSea5 is evaluated against ERA5 waves. We find that in ERA5 the seasonal and spatial variations of eastward-moving Kelvin wave activity are mainly determined by the ambient zonal flow, with wave activity being stronger in easterlies than westerlies. For the westward-moving mixed Rossby–gravity waves and equatorial Rossby waves, the seasonal and spatial variations of the upper-tropospheric wave activity are determined by both the ambient flow and extratropical forcing with stronger wave activity generally in the westerlies, whilst the lower-tropospheric wave activity is related to the ambient flow and tropical convection. In GloSea5, the Kelvin wave activity is not well simulated in the upper troposphere, and in general the wave activity and wave-related convective signal are too weak. In contrast, GloSea5 performs better for the westward-moving equatorial waves, including their Doppler-shifted eastward-moving components, despite a significant overestimation in the Atlantic and African region. The phase of ENSO has a substantial impact on equatorial waves in bothe ERA5 and GloSea5. The mechanism of the impact is through changes in the ENSO-related ambient flow, upper-tropospheric extratropical forcing, and tropical convection. GloSea5 can capture the low-level Kelvin wave–ENSO relationship reasonably well, with stronger wave activity over the eastern Pacific in El Niño, although the ENSO-driven variation is too weak. The wave–ENSO relationship for westward-moving waves is well represented in GloSea5, especially in the upper-level eastern-Pacific westerly duct region in the extended boreal winter and the low-level Indo-Pacific in all seasons. We conclude that in GloSea5 the representation of the wave–ENSO teleconnection is the key driver for the performance of interannual variability in the wave activity.

KEYWORDS

ambient zonal winds, ENSO, equatorial Rossby waves, equatorial wave activity, Kelvin waves, mixed Rossby–gravity waves, seasonal and interannual variations, tropical convection

1 | INTRODUCTION

Equatorially trapped waves are fundamental components of the tropical atmosphere. They are closely related to fundamental phenomena of the tropical climate and weather, such as the forcing of the equatorial quasi-biennial oscillation (QBO) and semi-annual oscillation (e.g. Lindzen and Holton, 1968; Baldwin *et al.*, 2001; Pahlavan *et al.*, 2021), the Walker circulation (e.g. Gill, 1980), and the El Niño–Southern Oscillation (ENSO: e.g. Lau, 1981; Yu and McPhaden, 1999). They are also found to contribute to atmospheric teleconnection patterns (e.g. Lim and Chang, 1983), the Madden–Julian oscillation (MJO: e.g. Lau and Peng, 1987; Masunaga, 2007; Roundy, 2008), and transient features of the Hadley cell (e.g. Hoskins *et al.*, 2020; Hoskins and Yang, 2021; Tomassini and Yang, 2022).

On the synoptic scale, the importance of equatorial waves for tropical convection has been recognised for several decades (e.g. Takayabu, 1994; Wheeler and Kiladis, 1999; Wheeler *et al.*, 2000; Yang *et al.*, 2007a, 2007b; Kiladis *et al.*, 2009; Ferrett *et al.*, 2020; Peatman *et al.*, 2021; Ayesiga *et al.*, 2022). Recently, the dynamical role of equatorial waves in high-impact weather, such as tropical extreme precipitation and tropical cyclones, has been highlighted from observations. Ferrett *et al.* (2020) showed that heavy precipitation in Southeast Asia is up to four times more likely when equatorial waves are strong and have their low-level convergence and cyclonic vorticity in phase with the precipitation. Yang *et al.* (2018) also revealed that westward-moving equatorial waves provide favourable conditions for the initiation of African Easterly waves. Recently, Feng *et al.* (2023) demonstrated that related to the effect on the large-scale environment such as divergence, cyclonic vorticity and humidity, equatorial waves can serve as useful precursors to the occurrence and intensification of tropical cyclones. Hence, equatorial waves can provide important sources of predictability for tropical high-impact weather.

Recent studies have shown that the main reason for the tropics having longer predictability (>20 days) than the higher latitudes is that equatorial waves are less prone to error growth than midlatitude baroclinic disturbances because of their periodicity and coherent phase propagation (e.g. Wheeler *et al.*, 2017; Judt, 2020; Li and Stechmann, 2020). Therefore, understanding and evaluating model performance for equatorial wave activity is important for improving high-impact weather forecasts in the tropics beyond a few days ahead; it is also likely to be important for climate (e.g. Lin *et al.*, 2006; Ringer *et al.*, 2006; Yang *et al.*, 2009; Hung *et al.*, 2013).

To understand the performance of seasonal forecasts in the tropics, it is crucial to evaluate a model's ability to represent the seasonal variation of equatorial wave activity and their interannual variation associated with ENSO. However, to the best of our knowledge, there has been no such study, as the vast majority of existing studies of equatorial waves are mainly on intraseasonal and synoptic time-scales. As well, these studies have focused on the equatorial wave-related convective variables filtered over a wave-number-frequency domain which is confined by the dispersion curves of equatorial waves (e.g. Wheeler and Kiladis, 1999; Kiladis *et al.*, 2009; Knippertz *et al.*, 2022). Convective signals are useful for investigating convectively coupled equatorial waves. However, to reveal the important dynamical impacts of equatorial waves on tropical high-impact weather, such as extreme precipitation and tropical cyclones, it is also essential to examine the associated winds of equatorial waves. Using solely convection-related information may lead to a failure to identify equatorial waves when and where they are not convectively coupled. Also, equatorial waves identified from the convective signal alone cannot be easily used to independently relate precipitation to the wave structure.

ENSO is the strong mode of the interannual variability in the ocean–atmosphere system. The studies of Yang and Hoskins (2013, 2016) showed that the ENSO phase has a substantial impact on equatorial wave winds, mainly through ENSO-induced changes in the thermal conditions, the ambient flow and the local zonally propagating forcing and remote forcing from the extratropics. In particular, the ENSO impact on Kelvin waves is mainly through changes in the tropical convection, and in the upper troposphere through the ambient zonal flow and associated extratropical forcing. On the other hand, ENSO impacts on westward-moving mixed Rossby–gravity and meridional mode number $n = 1$ Rossby waves are mainly through changes in the ambient flow and the associated extratropical forcing. Yang and Hoskins (2013, 2016) using data from the European Centre for Medium-Range Weather Forecasts (ECMWF) ERA-Interim reanalysis focused on the extended boreal winter and summer in the upper troposphere. It is valuable to fully examine the ENSO–wave relationship in all seasons and in both the upper and lower troposphere, using the latest reanalysis, the ECMWF fifth-generation climate reanalysis (ERA5: Hersbach *et al.*, 2020).

In this study, we use the method of projecting dynamical fields onto equatorial wave modes as developed in Yang *et al.* (2003) to identify equatorial waves in data from ERA5 and ensemble forecasts from the Met Office Global Seasonal Forecast System version 5 (GloSea5). The ERA5 waves are used as a benchmark for evaluation of the seasonal forecast performance. The purpose of this study is:

(i) to provide a systematic study of the seasonal variation and ENSO-related variation of dynamical equatorial wave activity, in both the ERA5 reanalysis and GloSea5 simulations; (ii) to increase our understanding of the behaviour of equatorial waves, including the impact mechanisms of the tropical ambient zonal flow and convective activity on equatorial wave behaviours; and (iii) to use the understanding as a solid benchmark to evaluate the model performance, shedding light on areas for model improvement.

The outline of the article is as follows. Section 2 gives a summary of the data used, the methodology for identifying the equatorial waves, and a brief description of the theories associated with the mechanisms involved in the impact of the ambient zonal flow on the equatorial waves. Section 3 starts by showing the seasonal ambient zonal winds, then the climatological seasonal variation and longitudinal distribution of equatorial wave activity and tropical convective activity, followed by the presentation of the impact of ENSO on the ambient zonal flow, tropical convection, and equatorial wave activity. A summary and discussion are given in Section 4.

2 | DATA, METHODOLOGY AND THEORY

2.1 | Datasets

The horizontal winds (u, v) and the geopotential height (Z) at 850 and 200 hPa are used to identify equatorial waves for both ERA5 and GloSea5 forecasts. The GloSea5 forecasts have seven ensemble members initialised four times per month (1st, 9th, 17th and 25th) yielding a 28-member ensemble each month. The data used are for the common period from 1993 to 2015 (the GloSea5 re-forecasts are only available for 1993–2015). The equatorial wave datasets contain the four greatest equatorial waves: eastward-moving Kelvin waves, westward-moving mixed Rossby–gravity (MRG) waves, and meridional mode number $n = 1$ and 2 equatorial Rossby (R1 and R2) waves. In this study, daily outgoing long-wave radiation (OLR) from the National Oceanic and Atmospheric Administration (NOAA) (Liebmann and Smith, 1996) and GloSea5 on a $2.5° \times 2.5°$ grid are used as a proxy for convection.

2.2 | Methodology to identify equatorial waves

The methodology developed in Yang *et al.* (2003) is used to identify the equatorial waves. The method does not assume that the linear adiabatic theory for equatorial waves on a resting atmosphere is directly applicable. In particular, the dispersion relation and vertical structure are not imposed, because in reality these aspects are sensitive to any background zonal flow that varies with height and time. Potential equatorial waves are identified by projecting u, v and Z in the tropics at each pressure level onto the different equatorial wave modes using their horizontal structures described by parabolic cylinder functions in the meridional direction and sinusoidal variation in the zonal direction. The basis functions used for the wave projection are orthogonal. For the parabolic cylinder functions, the meridional trapping scale is $y_0 = 6°$. The value of y_0 is pre-determined from a best fit of the theoretical equatorial wave solutions to observational data, where the structures of the equatorial waves are not sensitive to the choice of y_0 (Yang *et al.*, 2003, 2012). The same y_0 was also used in Gehne and Kleeman (2012). However, it should be noted that, in the real flow, waves with different y_0 may emerge and the methodology using only one y_0 would project all detected signal to the same meridional width. Also, as there is not a complete theory for equatorial waves in shear parallel flows, the untilted modes on a resting atmosphere are used as basis structures which are not expected to be exactly the same as normal modes of the real flow.

Although the spatial projection method can be applied to data without any time filter, before the projection, a broad-band spectral filter with wave-number 2–40 and period 2–30 days is applied to separate eastward- and westward-moving waves. The filter domain is generally wider than that which fits the usual shallow-water dispersion curves used in most studies of equatorial waves (Knippertz *et al.*, 2022). Therefore, the phase speed of the waves identified is not tightly constrained by the spectral filter. This allows features with different characteristic scales to be identified, and can account for Doppler shift of frequencies by the background zonal flow. The filter excludes wave-number-1 planetary waves. The lower cut-off of 2 days is to remove the diurnal cycle, and the upper cut-off of 30 days is to remove intraseasonal variability and beyond. More details of the methodology can be found in Yang *et al.* (2003, 2007a, 2012, 2018).

The methodology has been employed in various studies to investigate the connection of equatorial waves and various atmospheric phenomena, such as tropical convection, tropical cyclones, Hadley Cell, QBO and ENSO (e.g. Yang *et al.*, 2007a, 2007b, 2011, 2012, 2013, 2018; Ferrett *et al.*, 2020; Hoskins *et al.*, 2020; Hoskins and Yang, 2021; Peatman *et al.*, 2021; Ayesiga *et al.*, 2022; Tomassini and Yang, 2022; Feng *et al.*, 2023). The methodology has also been applied to numerical simulations (e.g. Yang *et al.*, 2009; Ayesiga *et al.*, 2022; Ferrett *et al.*, 2023) and real-time global operational numerical weather prediction (NWP) forecasts and hybrid dynamical-statistical forecasts (Yang *et al.*, 2021; Ferrett *et al.*, 2023).

To investigate the wave activity, the standard deviation (SD) of daily wave winds is calculated for each wave mode for each month. Seasonal wave activity is represented by the 3-month mean of the monthly SD. For GloSea5, the SD is computed for each ensemble member. The behaviour of the seasonal mean equatorial wave activity in GloSea5 does not substantially change with the forecast lead time (not shown), therefore we only show results for forecasts at a lead time of 2 months. Any substantial deviations from these results at lead times of 1 and 3 months are described in the text only.

It is noted that since the zonal wind of the Kelvin wave and meridional wind of MRG, R1 and R2 waves can represent their meridional structures for the wave, wave activity is represented by these variables at a given latitude. The selected latitude varies depending on the wave mode, and is chosen to capture the peak of wave activity: 0° for Kelvin wave and MRG wave, 8°N for R1 wave and 13°N for R2 wave. As the meridional structures of the waves are strictly defined by the parabolic cylinder functions, our results do not depend on the choice of latitude.

2.3 | Theories associated with mechanisms of the ambient flow impact on equatorial waves

To understand the activity of equatorial waves, it is useful to give a succinct review of the theories associated with mechanisms that may influence the occurrence and behaviour of equatorial waves. More details of the mechanisms have been given in Yang and Hoskins (2016) and Hoskins and Yang (2016). The mechanisms are closely related to the tropical ambient zonal flows. Briefly, the ambient zonal flow can determine the following four aspects of equatorial waves, mainly through the Doppler-shifting effect.

2.3.1 | The existence of free equatorial waves

Equatorial wave theory states that the Kelvin waves propagate eastward relative to the mean ambient zonal flow (U), and MRG and equatorial Rossby waves propagate westward relative to the ambient zonal flow, therefore waves with zonal phase speed c exist only in zonal winds that satisfy

$$c - U > 0 \text{ for Kelvin waves and,} \tag{1}$$

$$-\beta/k^2 < c - U < 0 \text{ for MRG and Rossby waves.} \tag{2}$$

Kelvin waves only exist in regions of easterly or weak westerly winds in which they have an eastward phase speed with respect to the ambient flow. Westward-moving MRG, R1 and R2 waves only exist in regions of westerly or weak easterly winds in which they have a westward phase speed with respect to the ambient flow whose magnitude should not be larger than β/k^2.

2.3.2 | The change in the energy of equatorial waves following their zonal propagation in a zonally varying flow

In Hoskins and Yang (2016) the theory for one-dimensional propagation of waves in a longitudinally varying zonal flow was developed. The theory states that the wave energy (E) variation along a ray path is given by

$$\frac{d\ln E}{dx} = -\frac{B}{c_g}\frac{dU}{dx}, \tag{3}$$

where

$$B = 1 + \frac{c_{gi}}{c_i} - \frac{k}{c_g}\frac{\partial c_{gi}}{\partial k}, \tag{4}$$

where c_{gi} is the intrinsic group velocity, $c_g = c_{gi} + U$ is the absolute group velocity, and c_i is the intrinsic phase speed.

The behaviour of the energy for equatorial waves depends on the sign and magnitude of B and c_g, which varies with the property of the wave considered and the structure of the ambient zonal flow. For non-dispersive Kelvin waves, $c_i = c_{gi}$, B reduces to 2, hence Equation (3) becomes a simple analytical form:

$$E = E_0\left|\frac{U_0 + c_{gi}}{U + c_{gi}}\right|^2, \tag{5}$$

where E_0 is the energy at a given longitude at which $U = U_0$. Equation (5) states that the energy variation of the Kelvin wave along a ray path is in the opposite sense to that of U, with a maximum occurring in a minimum (relative easterly) of U. For dispersive MRG and R1 waves, the energy variation along a ray is more complicated as indicated in Equations (3) and (4), and there are no analytical solutions. More detailed analysis of various wave modes can be found in Hoskins and Yang (2016).

2.3.3 | The response of equatorial waves to a zonally propagating forcing

As in Zhang (1993) and Hoskins and Yang (2000), considering the forcing of an equatorial wave with a natural (intrinsic) frequency, ω_k, by a forcing with frequency ω_f, if the wave is Doppler shifted by a basic flow U with the Doppler-shifted frequency $\omega k = \omega k + kU$, then in the

presence of damping α, the magnitude of the response will depend on the intensity of the forcing and on the amplification A defined as follows:

$$A = \frac{1}{|\omega_f - \tilde{\omega}_k - i\alpha|} = \frac{1}{\left\{\left[\omega_f - (\omega_k + kU)\right]^2 + \alpha^2\right\}^{1/2}}. \quad (6)$$

Provided that the damping is not too large, the nature of the response will tend to be dominated by the waves that are close to resonance. For ambient zonal winds in the real atmosphere, the Kelvin wave response is generally larger in easterlies than in westerlies, and larger for eastward-moving (positive frequency) forcing than westward-moving forcing. In contrast, the response for the MRG, R1 and R2 waves is generally larger in westerlies than in easterlies.

2.3.4 | The extratropical forcing through Rossby waves propagation

As linear theory states that Rossby waves always propagate westward relative to the mean flow, stationary and eastward-moving extratropical Rossby waves can only propagate into low latitudes in regions of mean westerly flow (Charney, 1969; Yang and Hoskins, 1996). Observed extratropical forcing of equatorial waves has been found predominantly in the Western Hemisphere upper-tropospheric equatorial westerly ducts over the eastern Pacific and Atlantic, especially in the boreal winter (e.g. Webster and Holton, 1982; Kiladis, 1998; Yang *et al.*, 2007c; Yang and Hoskins, 2013, 2016).

Although it was believed that equatorial easterlies can inhibit extratropical Rossby waves from propagating into the tropics due to the existence of critical lines, a few studies show that extratropical Rossby waves with westward-moving phase speed can propagate into the equatorial easterly region to excite westward-moving equatorial waves (e.g. Yang and Hoskins, 1996; Yang *et al.*, 2018). In addition to the forcing associated with the meridional propagation of extratropical disturbances, extratropical Rossby waves can remotely or laterally excite equatorial waves (e.g. Magaña and Yanai, 1995; Hoskins and Yang, 2000; Straub and Kiladis, 2003; Yang and Hoskins, 2013; Kiladis *et al.*, 2016; Tulich and Kiladis, 2021; Cheng *et al.*, 2022).

The above mechanisms suggest that in general an easterly flow is favourable for Kelvin wave activity and a westerly flow is favourable for the westward-moving equatorial waves. This is also exhibited in some modelling studies (e.g. Wang and Xie, 1996; Hoskins and Yang, 2000). These impacts are expected to be stronger in the upper troposphere where the zonal mean flow and extratropical forcing are stronger than those in the lower troposphere.

3 | RESULTS

3.1 | Seasonal and longitudinal distributions

3.1.1 | Tropical ambient zonal flow

Before showing the equatorial wave activity, it is useful to first examine the tropical ambient zonal flow since it is fundamentally important for the occurrence and behaviour of equatorial waves as discussed in Section 2.3. Figure 1a shows the geographical distribution of the climatological seasonal mean zonal winds at 200 hPa for June–August (JJA) and December–February (DJF) in ERA5 and GloSea5. In ERA5, in the upper troposphere, there are strong easterlies in the Eastern Hemisphere (EH) in the boreal summer associated with the Asian summer monsoon and strong westerlies in the Western Hemisphere (WH) in the boreal winter associated with the two well-known equatorial westerly ducts (e.g. Webster and Holton, 1982). In general, GloSea5 produces a seasonal mean zonal wind distribution similar to that in ERA5. However, GloSea5 has a clear westerly bias in the upper troposphere over the tropical Atlantic extending to Africa, especially in boreal summer where the westerly bias is up to 10 $m \cdot s^{-1}$. Figure 1b,c shows the seasonal mean (3-month moving average) of near-equatorial zonal winds averaged over 15°N–15°S at 200 and 850 hPa, respectively. The upper-tropospheric westerly bias over the Atlantic in GloSea5 is clearly seen in Figure 1b. The westerly duct in the eastern Pacific in GloSea5 is also stronger, and shifted eastward, compared to ERA5. Furthermore, the easterlies in the EH are weaker, and shifted eastward, compared to ERA5. In the lower troposphere, the zonal winds in ERA5 and GloSea5 (Figure 1c) have a reversed sign from those in the upper troposphere, as a feature of Walker circulations. In GloSea5, the low-level easterly is underestimated over the central-eastern Pacific and slightly overestimated in the Atlantic.

3.1.2 | Kelvin waves

Figure 2 shows the seasonal Kelvin wave activity at 200 and 850 hPa. Consistent with the theoretical mechanisms mentioned in Section 2.3, in ERA5 the Kelvin wave amplitude (Figure 2a,d) tends to reach the maxima when and where the background mean flow is relative easterlies (Figure 1b,c), such as in the Indian Ocean for all seasons

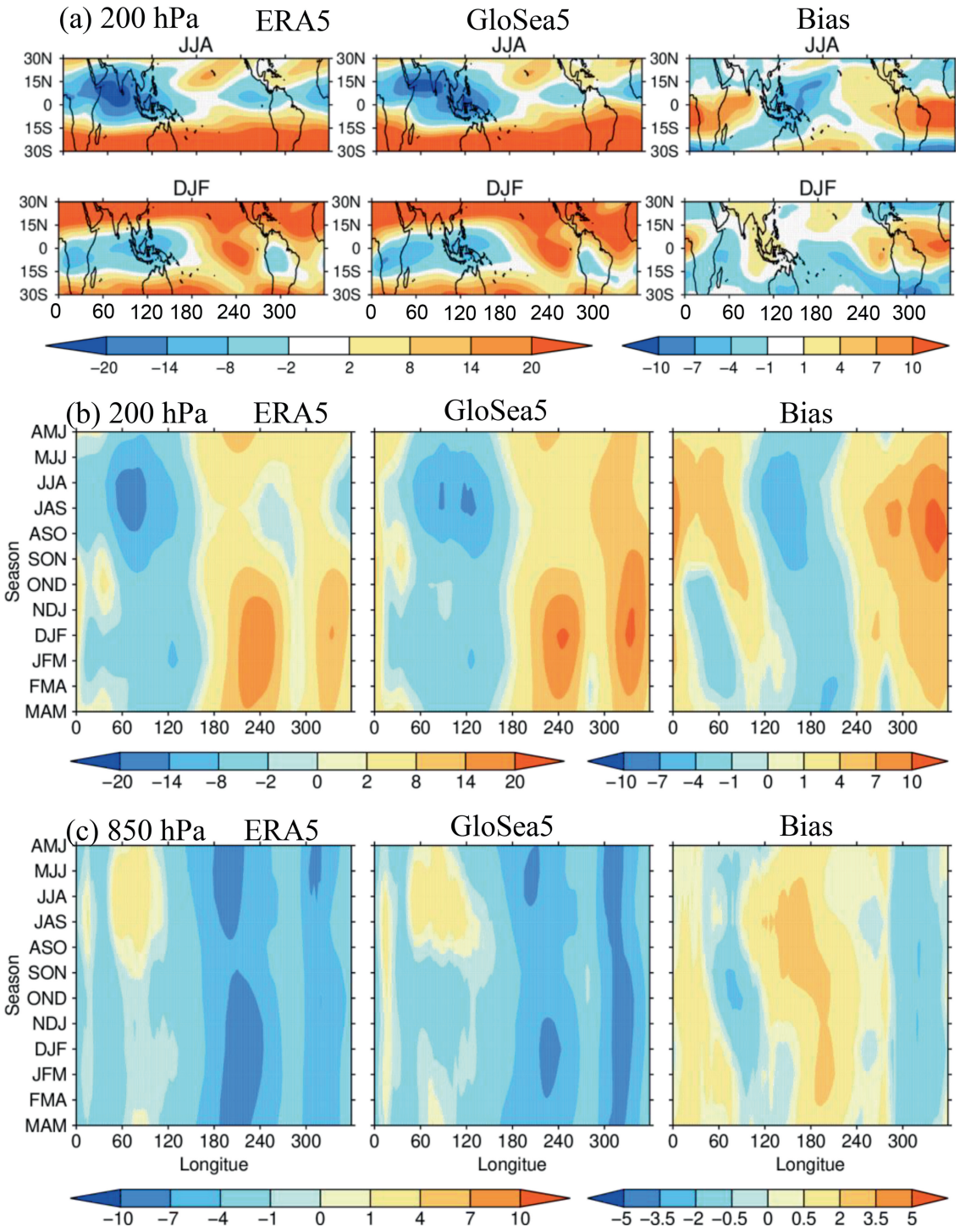

FIGURE 1 In 1993–2015, (a) seasonal mean of ambient zonal wind U (m·s^{-1}) at 200 hPa in JJA and DJF, (b,c) equatorial (15°N–15°S) U at (b) 200 hPa and (c) 850 hPa for all seasons, for ERA5 (left), GloSea5 reforecast ensemble mean (middle), and the GloSea5 Month 2 bias (GloSea5 minus ERA5; right).

and also in a narrow region over the eastern Pacific in boreal summer at 200 hPa (Figure 1b), and in the central-eastern Pacific at 850 hPa (Figure 1c). It is worth noting that the two narrow peaks at 850 hPa over the Andes and Eastern Africa are associated with the topography (Figure 2d).

GloSea5 (Figure 2b) does not well predict the upper-level Kelvin wave activity and the wave relationship with the ambient flow (Figure 1) as seen in ERA5 and suggested by the theoretical mechanisms in Section 2.3. In GloSea5, the peak of Kelvin wave activity over the easterly region of the Indian Ocean only appears in certain

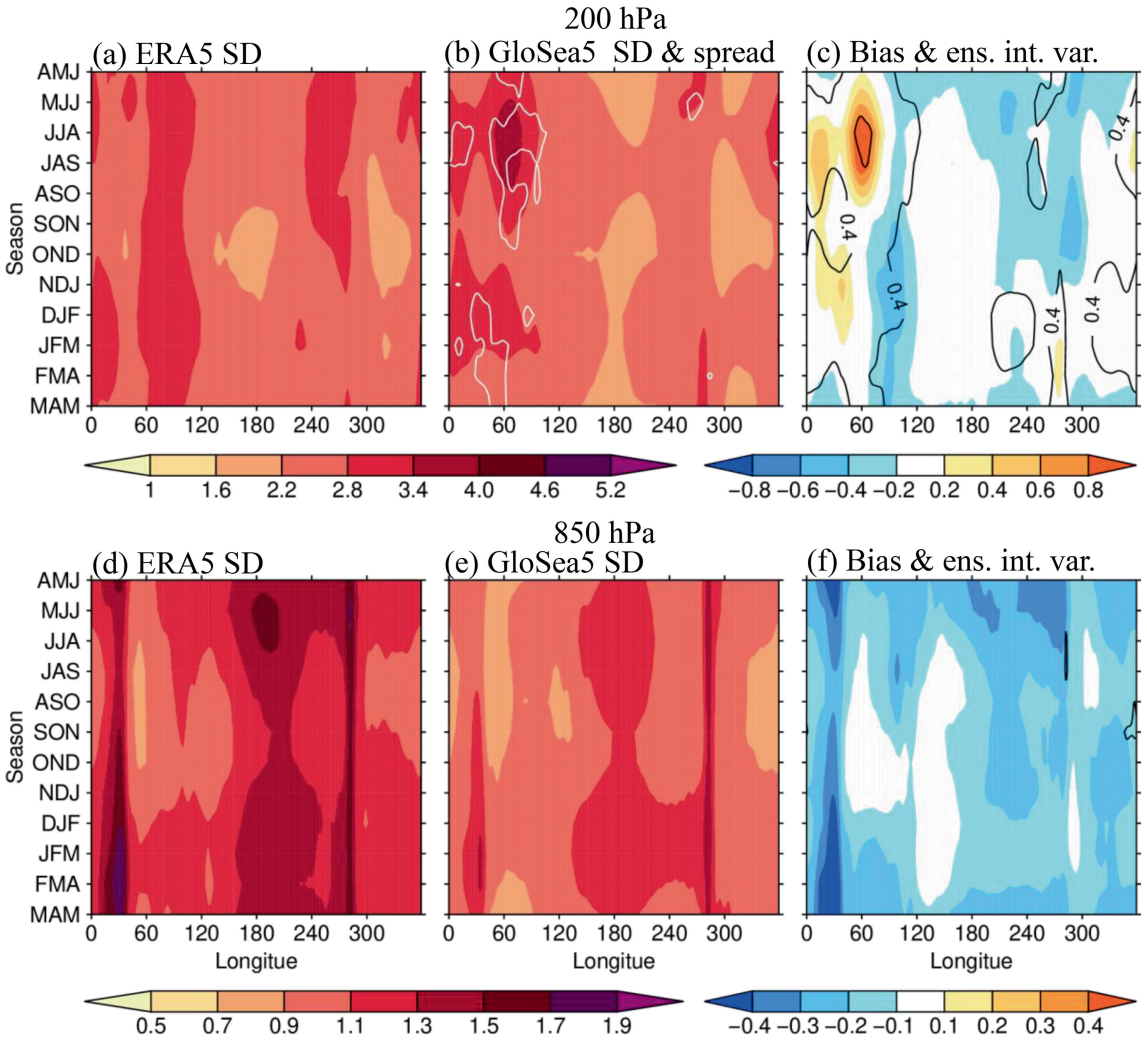

FIGURE 2 Climatology (1993–2015) seasonal mean of Kelvin wave activity (SD of equatorial u, unit m·s^{-1}) in ERA5 (left), GloSea5 Month 2 reforecast ensemble mean (FC) (middle), and the GloSea5 Month 2 bias (right), at (a–c) 200 hPa and (d–f) 850 hPa. White contours in (b) are the ensemble spread, with the contour interval of 0.1 m·s^{-1}. At 850 hPa the spread is less than 0.05 m·s^{-1} so contours not shown. In (c,f), the black contours indicate the ensemble mean of the interannual variability in each member, with a contour interval of 0.2 m·s^{-1} at 200 hPa and 0.1 m·s^{-1}at 850 hPa, which are the same intervals as for the colours.

seasons, and also shifts westwards compared with that in ERA5. The wave activity is underestimated over a large longitude sector from the eastern Indian Ocean to the Atlantic. At 850 hPa, the seasonal and longitudinal pattern of the Kelvin wave activity and its connection with the ambient zonal flow are better simulated in GloSea5, with the wave activity peaking in the central-eastern Pacific where there are easterlies. However, the wave amplitude remains underestimated in most seasons and regions.

At both levels, the model ensemble spread (white line contours in the middle column in Figure 2) is small. At 200 hPa, the largest ensemble spread is only about 3% of the mean over east Africa–west Indian Ocean in the extended boreal summer where the bias is large (Figure 2c). The ensemble interannual variability, defined as the mean of the interannual variability over all individual members (black contours in Figure 2c,f), is about 0.4 m·s^{-1} in various regions at 200 hPa and less than 0.2 m·s^{-1} at 850 hPa.

3.1.3 | MRG waves

Figure 3 shows the MRG wave activity. The upper-level wave activity in ERA5 (Figure 3a) is strong over the eastern Pacific and Atlantic westerly duct regions (see Figure 1), especially in the extended boreal winter. This confirms the theoretical mechanisms that the westerly duct favours extratropical Rossby waves to propagate equatorward, likely triggering MRG waves (Yang and Hoskins, 2016). Consistent with the first and second mechanisms discussed in Section 2.3, the upper-level MRG (Figure 3a) has

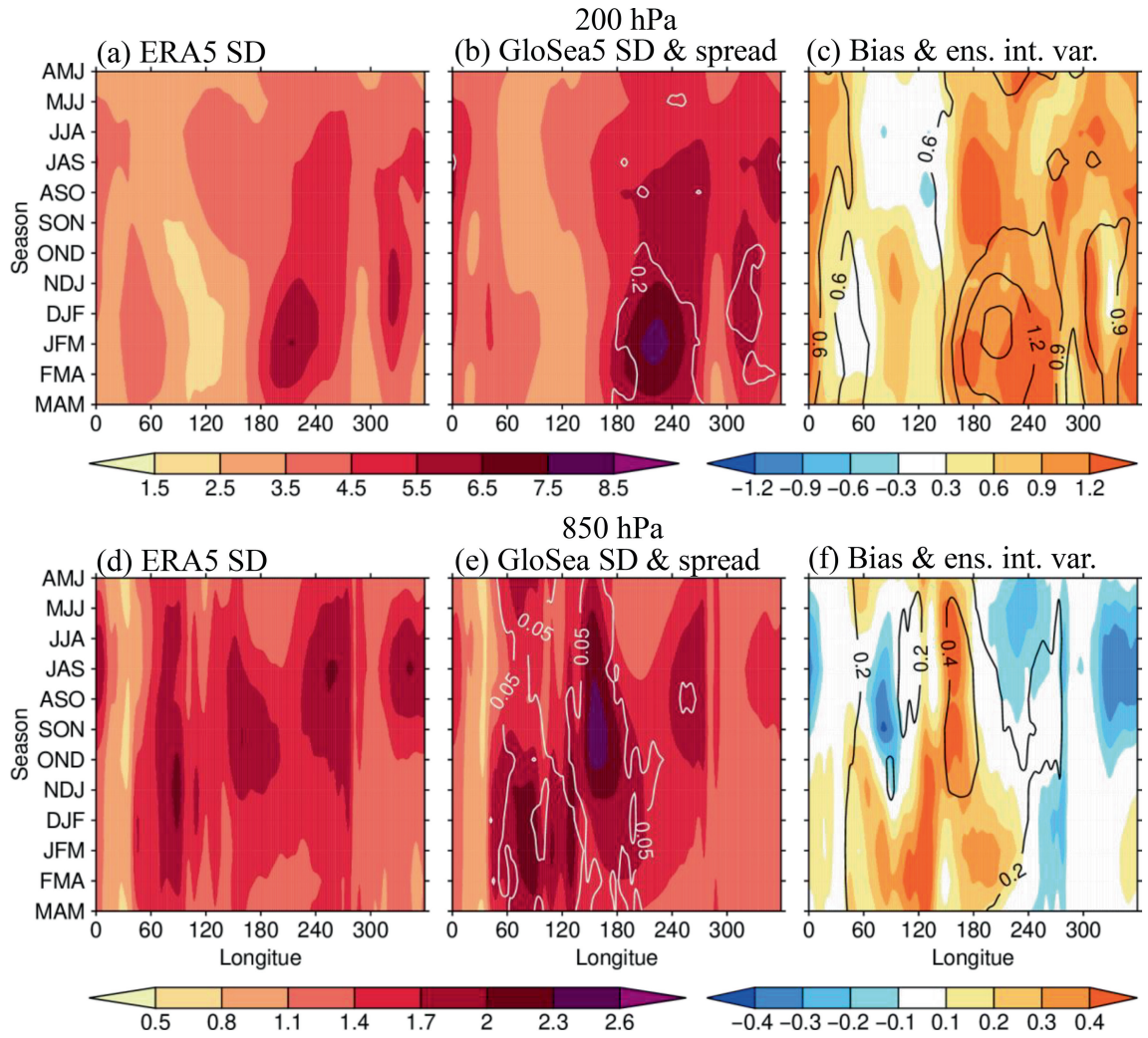

FIGURE 3 (a–f) As in Figure 2 but for MRG wave v on the Equator and in (c, f), the black contour interval is 0.3 m·s^{-1} at 200 hPa and 0.2 m·s^{-1} at 850 hPa.

the minimum amplitude over the Indian–western Pacific where there are easterlies. GloSea5 predicts well the features of the upper-level MRG activity in the EH, whilst the wave amplitude is overestimated in the WH (Figure 3b,c). The bias over the eastern Pacific and Atlantic is related to the westerly bias there (Figure 1b), as too strong westerlies are expected to allow more extratropical disturbances to propagate equatorwards to excite equatorial waves. On the other hand, the bias in the central Pacific, especially in boreal summer and autumn, is likely related to too strong westward-moving convective activity in the central Pacific (will be shown later in Figure 7b).

At 850 hPa, the MRG activity in ERA5 (Figure 3d) also shows some connections with the ambient flow, with strong wave activity generally appearing in relative westerly regions. On the other hand, as the strong activity is over the oceanic sectors (the Indian Ocean in all seasons, the Pacific and Atlantic in boreal summer and autumn), it is suggested that the low-level MRG waves are also associated with the thermal condition such as convection. The GloSea5 forecasts (Figure 3e) can capture the seasonal and longitudinal distribution of the low-level waves, but there are some magnitude biases. Strong bias occurs in the Indo-Pacific region (Figure 3e,f). In the extended boreal summer, GloSea5 overestimates wave activity in the western Pacific around 150°E, but underestimates the wave activity in the eastern Indian Ocean, whereas in the extended boreal winter, GloSea5 generally overestimates wave activity in the Indo-Pacific region. Some underestimation is also seen in the eastern Pacific and Atlantic in the extended boreal summer. It is interesting that the low-level MRG wave bias in the Indo-Pacific region resembles the bias in the ambient zonal flow (Figure 1c, right panel), with westerly bias coincident with too strong wave activity, and the opposite is true. As will be shown later, the low-level MRG bias in the Indo-Pacific also resembles the bias of the westward-moving convective activity.

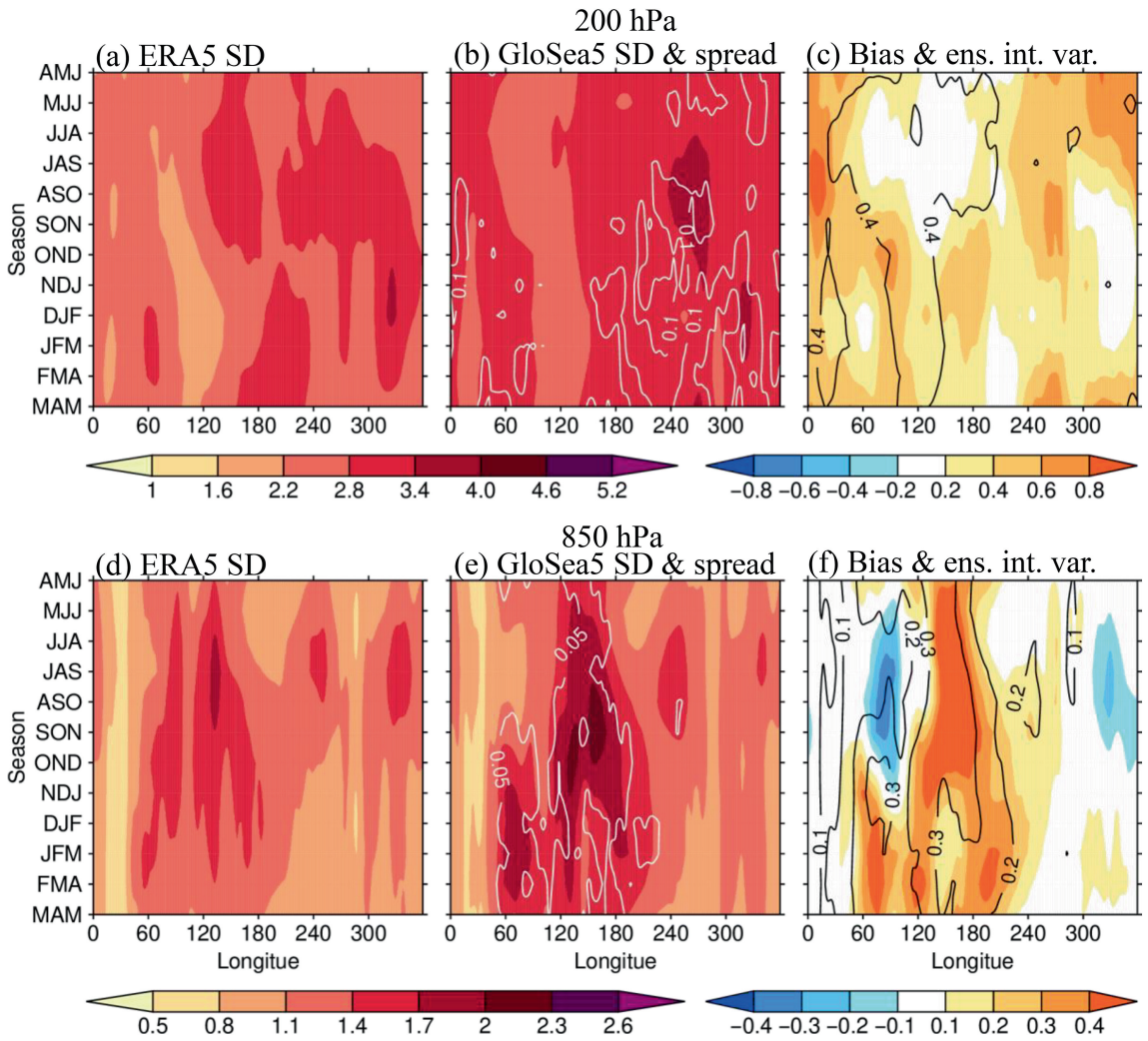

FIGURE 4 (a–f) As in Figure 2 but for R1 wave v at 8°N.

The ensemble spread of MRG wave activity in GloSea5 is small at 200 hPa, with a largest spread of 0.2 $m \cdot s^{-1}$ (about 4% of the ensemble mean) over the boreal winter westerly ducts where the ensemble interannual variation is comparable to the ensemble-mean bias. At 850 hPa, the ensemble spread is negligible (<0.1 $m \cdot s^{-1}$). The low-level ensemble interannual variability is largest over the western Pacific in the extended boreal summer, collocated with the large wave activity and large bias there.

3.1.4 | R1 and R2 waves

Figure 4 shows the R1 wave activity in ERA5 and GloSea5. At 200 hPa, the R1 wave activity in ERA5 (Figure 4a) also has a strong amplitude over the two westerly ducts in the extended boreal winter, despite it being less noticeable compared with that of the MRG. This is because the R1 waves, which have lower frequency than MRG as suggested by wave theory, are more easily Doppler-shifted to move eastwards in the westerly ducts, resulting in weaker westward-moving wave activity. More details will be discussed in the next subsection. In the extended boreal summer, the R1 wave activity is strong from the western Pacific to the Atlantic. As in the case of the MRG, the upper-level R1 activity is weakest in the Indian Ocean to western Pacific easterly region in most seasons. The upper-level R1 in GloSea5 shows less seasonal and longitudinal variations than in ERA5, and there are no clear maxima over the two westerly ducts in boreal winter (Figure 4b). However, GloSea5 can capture the R1 wave minima in the easterly region of the eastern Indian Ocean to western Pacific. In GloSea5, the upper-level R1 wave activity is also too strong over the Atlantic and East Africa in boreal spring and summer (Figure 4c). Noticeable ensemble interannual variability occurs over EH extended boreal summer where the wave bias and ensemble spread are small.

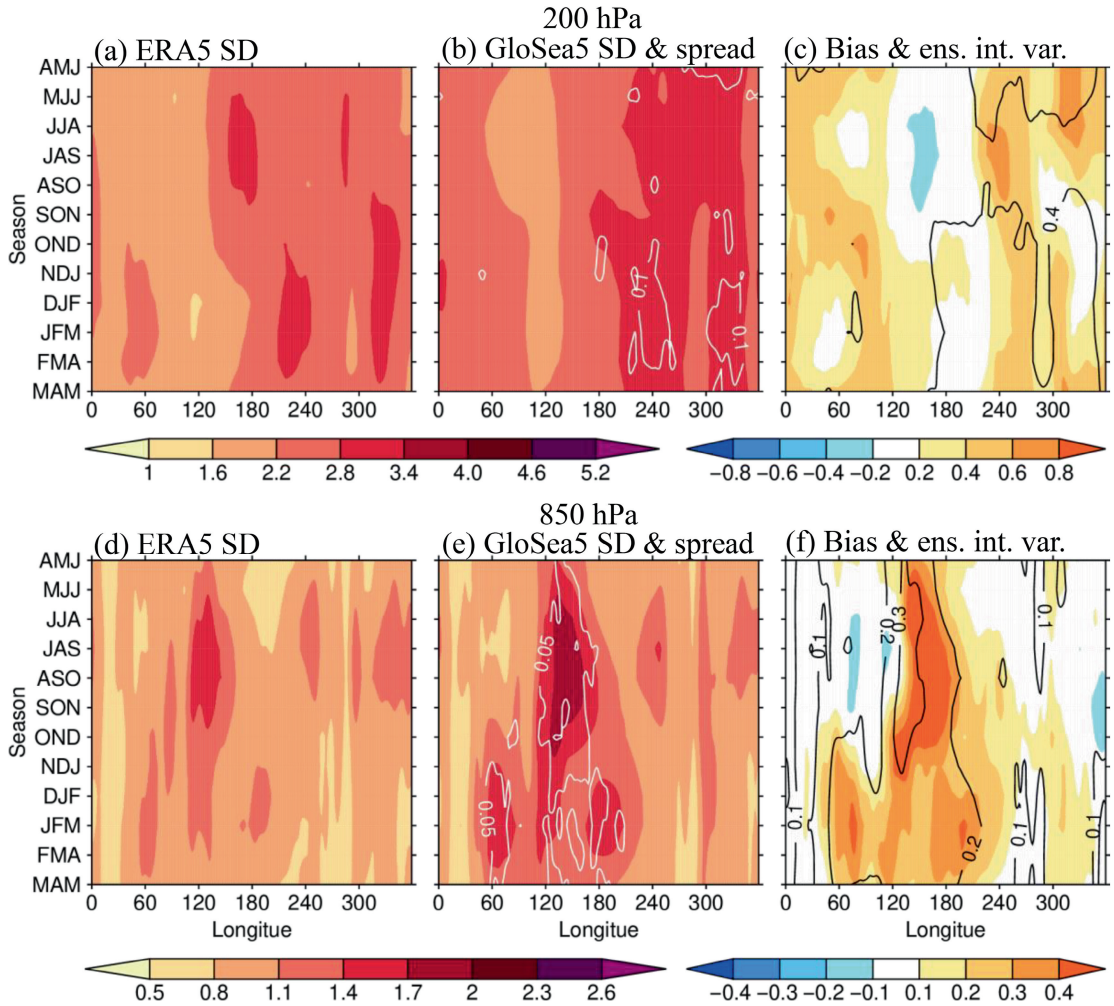

FIGURE 5 (a–f) As in Figure 2 but for R2 wave v at 13°N.

The low-level R1 wave activity in ERA5 (Figure 4d) shows similar distribution to that of the MRG, with strong activity over the Indian Ocean and western Pacific in most seasons, and over the eastern Pacific and Atlantic in boreal summer, but the activity peak over the western Pacific is shifted westward compared to that of the MRG. In GloSea5, the low-level R1 activity (Figure 4e) shows a generally consistent pattern with that in ERA5, but has a similar bias to that of the MRG in the Indo-Pacific sector (Figure 4f); whereas the underestimation bias in the eastern Pacific and Atlantic in the extended boreal summer is less clear. The low-level ensemble spread is small ($\sim$0.05 m·s^{-1}) and the large ensemble interannual variability appears where the wave activity is strong. R2 waves (Figure 5) have very similar seasonal and regional patterns to those for the R1 waves both in ERA5 and GloSea5, and exhibit a similar bias to that of the R1 except that there is no clear underestimation bias in the Indian Ocean in the extended boreal summer.

The common bias in the lower troposphere with too strong wave activity in the western Pacific seems to be consistent with the overestimation of tropical cyclone frequency in GloSea5 (Feng *et al.*, 2020), as westward-moving equatorial waves can largely affect the generation of tropical cyclones (Feng *et al.*, 2023).

3.1.5 | Eastward-moving Doppler-shifted MRG-E and R1-E in the upper troposphere

Previous observational studies show that the ambient zonal flow can lead to the Doppler shifting of equatorial waves (e.g. Yang *et al.*, 2007b; Dias and Kiladis, 2014; Yang and Hoskins, 2016). In particular, the strong westerly flow in the upper troposphere in the WH can lead MRG and R1 waves to move eastward. These waves remain the original wave structures but move eastward. Therefore, they are referred to as "MRG-E" and "R1-E" as suggested in Yang and Hoskins (2016).

To demonstrate the Doppler shifting effect, Figure 6a shows the dispersion curves for the three greatest wave modes ($n = -1$ Kelvin, $n = 0$ MRG and $n = 1$ R1) in a resting

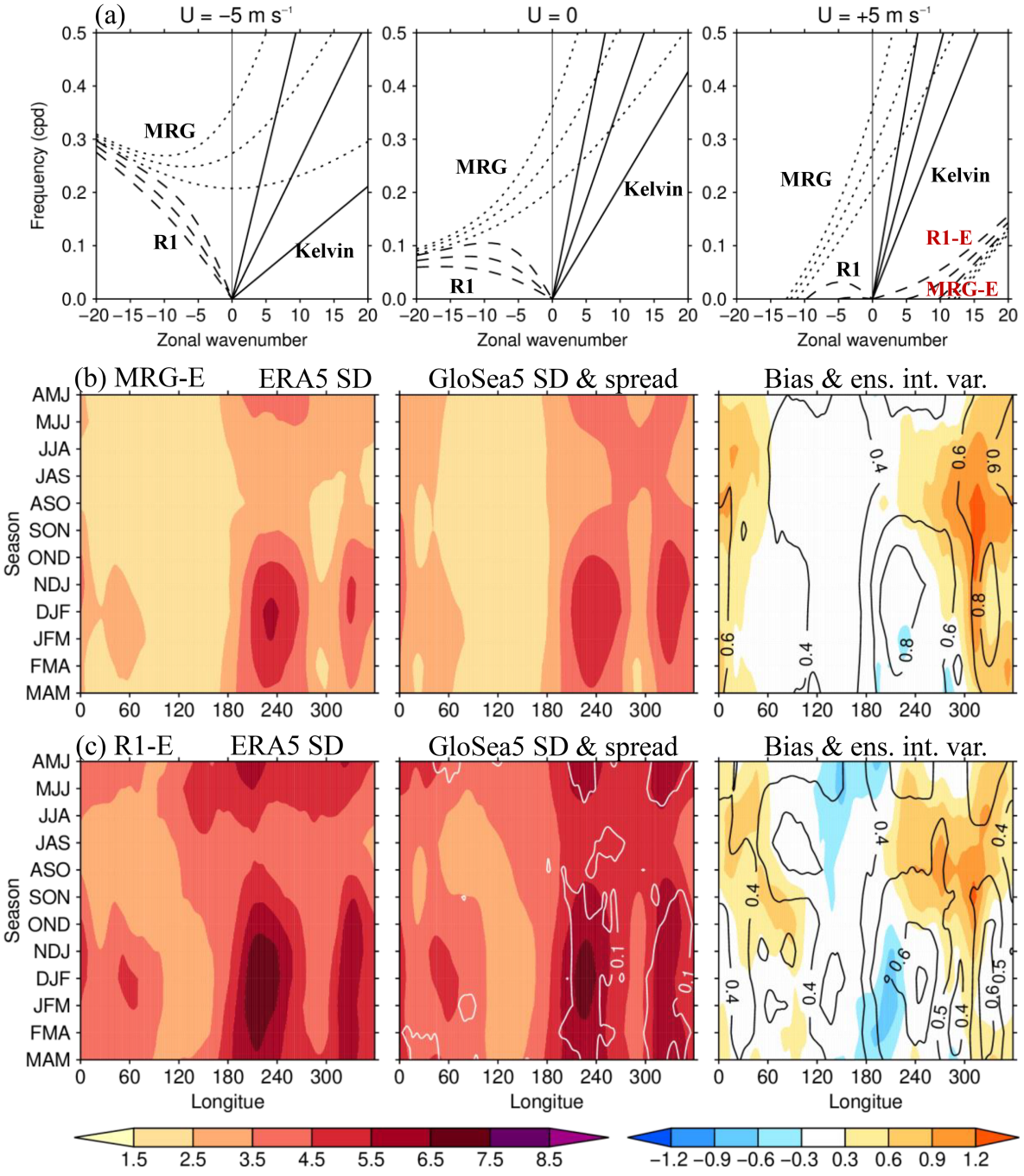

FIGURE 6 (a) Dispersion diagrams of the three greatest equatorial waves with equivalent depths of 10, 30 and 90 m, for $U = -5$, 0 and 5 m·s^{-1}. Eastward-moving waves have positive zonal wave-number k and westward-moving waves have negative k, for the Kelvin (solid), MRG (dotted) and R1 (dashed). (b, c) As in Figure 2a–c but for 200 hPa eastward-moving (b) MRG-E, and (c) R1-E. The black contours in the right panels have intervals of 0.2 m·s^{-1}.

atmosphere and with an ambient zonal wind of −5 and +5 m·s^{-1}. Compared to the resting atmosphere, an easterly flow leads the eastward-moving Kelvin waves to shift to lower frequencies, but leads westward-moving MRG and R1 to shift to higher frequencies. In a westerly flow, the Doppler shifting effect is reversed. However, with a westerly flow, smaller scale (large k) MRG and R1 waves which have lower frequencies are shifted to move eastwards. This is more obvious for the R1 waves as their frequency is lower than that of the MRG.

Figure 6b,c show the wave activity for the $n = 0$, 1 wave modes filtered over the eastward-moving k-ω domain. In both ERA5 and GloSea5, the two eastward-moving waves preferentially occur over the two westerly ducts in the WH. Comparing the observed eastward-moving waves with their westward-moving counterparts (MRG

in Figure 3a and R1 in Figure 4a) shows that over the two regions MRG-E is weaker than MRG, and in contrast R1-E is stronger than R1, consistent with the theory that the R1 waves are more likely Doppler-shifted by the westerly flow than the MRG. Glosea5 simulates the two eastward-moving waves reasonably well, except in the Atlantic and in the downstream (eastward-moving) Africa region, where as for the MRG and R1 their amplitudes are overestimated, related to the strong westerly bias there.

3.1.6 | Tropical convection

Since equatorial waves can be coupled to tropical convection (e.g. Wheeler and Kiladis, 1999; Yang *et al.*, 2007a, 2007b; Kiladis *et al.*, 2009; Ferrett *et al.*, 2020; Knippertz *et al.*, 2022), the behaviour of tropical convective activity is examined here. The geographic distribution of the seasonal mean and the standard deviations of NOAA OLR (Figure S1) indicates that the observed maximum convection (low OLR and large SD) is over the Indo-Pacific warm-pool region, and has two secondary maxima over central South America and Africa. These features are well captured by GloSea5. However, GloSea5 has a bias over the Indo-Pacific convective regions with the OLR activity being stronger (lower OLR and larger SD) than observed, especially in JJA and September–November (SON).

To examine the fraction of large-scale variability associated with the transient, propagating tropical convection, the OLR is separated into westward- and eastward-moving components in the same zonal wave number and frequency domain as that for the dynamical waves. Figure 7 shows the distribution of OLR standard deviation of the two components. For the eastward component (Figure 7a), GloSea5 tends to have an underestimation in most near-equatorial regions, especially in March–May (MAM) and JJA, and have an overestimation in the off-equatorial ocean basins (10–30°N and 10–30°S). In contrast, the westward-moving component of convective activity (Figure 7b) is far too strong in GloSea5, predominantly over most of the ocean basins and seasons, except in the Indian summer monsoon region. The seasonal westward-moving OLR SD averaged over 15°N–15°S (Figure S2) is generally too strong in the Indo-Pacific region in GloSea5, except in the Indian Ocean in the extended boreal summer where the westward-moving convection is too weak. Comparing the bias in the westward-moving convective activity (Figure S2, right panel) with the biases for the westward-moving waves at 850 hPa (Figures 3d, 4d and 5d), it is indicated that in the Indo-Pacific region the too strong convective activity is coincident with too strong westward-moving wave activity and vice versa. This suggests a strong convective coupling in the low-level waves.

Space–time power spectral analysis (Hayashi, 1982) is further performed to investigate the convective variability at different spatial and time scales. Figure 8 shows the OLR raw power spectra averaged over 15°N–15°S for the EH. Compared with observations, GloSea5 power is too strong at lower frequency, especially for the westward-moving component, but too weak in the eastward-moving higher frequency band. The deficiency in the Kelvin wave band is clearly seen in MAM and JJA even for the raw power (Figure 8c), and a too weak MJO signal is also shown except in September–November (SON). The raw power for the WH (Figure S3) also indicates similar model biases, but the magnitude of the bias in the lower frequency band is smaller than that in the EH.

Figure 9 further gives the power spectra with the background red spectrum removed as described in Wheeler and Kiladis (1999), for the EH and WH. This normalization procedure clearly highlights the spectral peaks associated with various equatorial waves in NOAA and GloSea5 with respect to their climatological variances. The power spectra for the NOAA OLR (Figure 9a,b) show that in all seasons and in both hemispheres, there are prominent spectral peaks in the eastward-moving component which are consistent with the theoretical dispersion curves of Kelvin waves for various equivalent depths. A peak can be seen in the lower frequency band associated with the MJO. It should be noted that the peak at $k = 14$ and period of about 9 days is caused by the sampling occurring in 14 swaths of satellite around the globe, as described in Wheeler and Kiladis (1999). In GloSea5, only SON and DJF show a weak Kelvin wave peak in the WH (Figure 9c,d), whereas in all other cases the Kelvin wave peak is entirely missing. This is consistent with the weak eastward-moving equatorial OLR SD shown in Figure 7. In contrast, GloSea5 is able to reproduce the westward-moving spectral peaks associated with MRG and R1, except there is an overestimation in MAM and DJF for both hemispheres.

It is also shown that in observations the power spectra associated with westward-moving tropical depressions ($k = 10\sim15$ and period = 3∼5 days) are stronger in JJA and SON for both hemispheres, whereas in GloSea5 the corresponding power spectra are too strong in MAM and DJF in both hemispheres but too weak in SON in the WH.

The weak convective signal in the Kelvin wave band is consistent with the weak Kelvin wave winds in GloSea5. The better performance of westward-moving convective activity in GloSea5 is also consistent with its better simulation of MRG and R1 wave winds. The limited skill of GloSea5 in simulating the Kelvin wave-related convection and the better performance in simulating the MRG and R1 wave-related convection was also shown for the

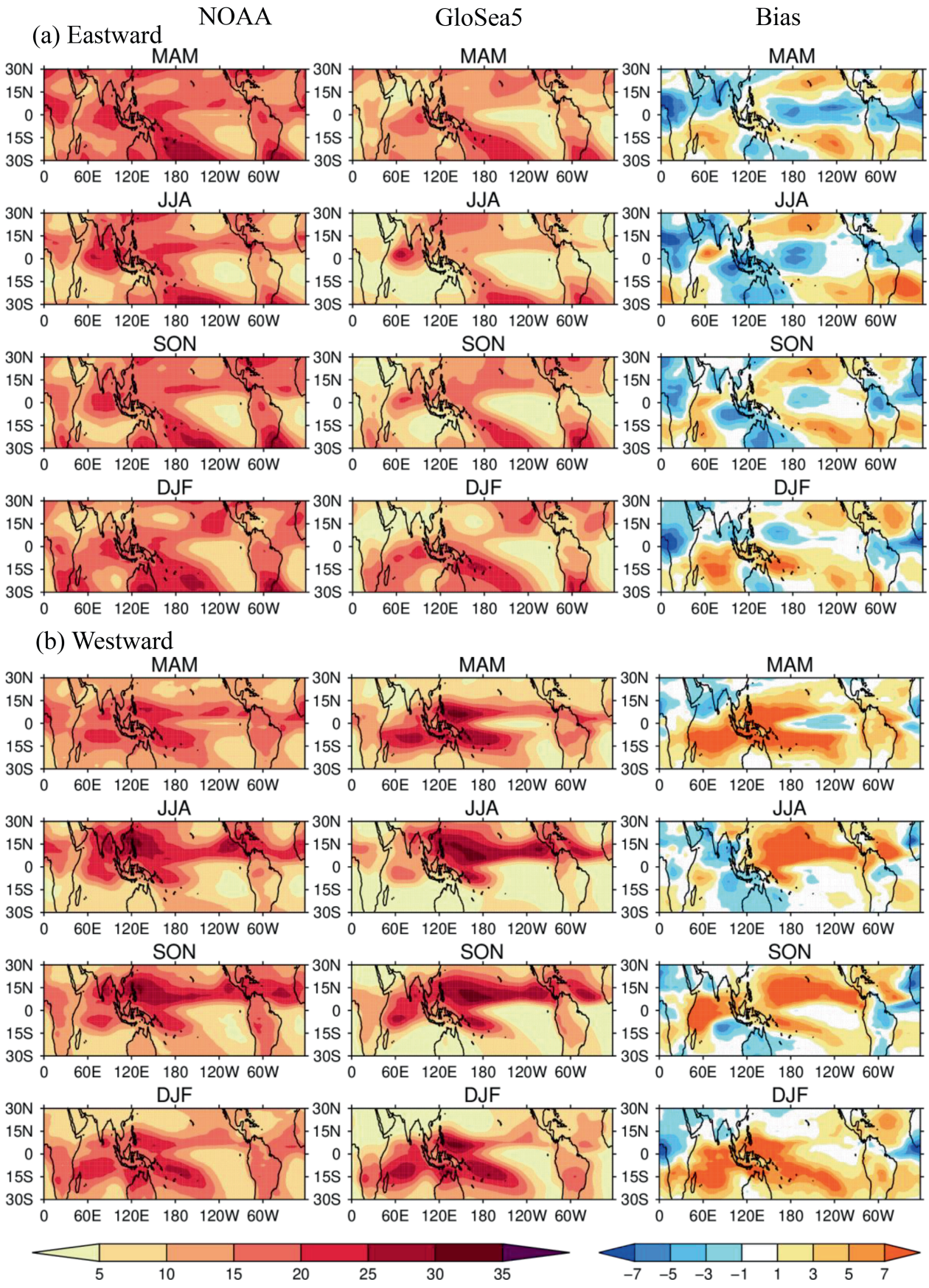

FIGURE 7 Seasonal standard deviations of OLR ($W \cdot m^{-2}$) for (a) eastward-moving component and (b) westward-moving component in (left) NOAA, (middle) GloSea5 and (right) GloSea5 bias.

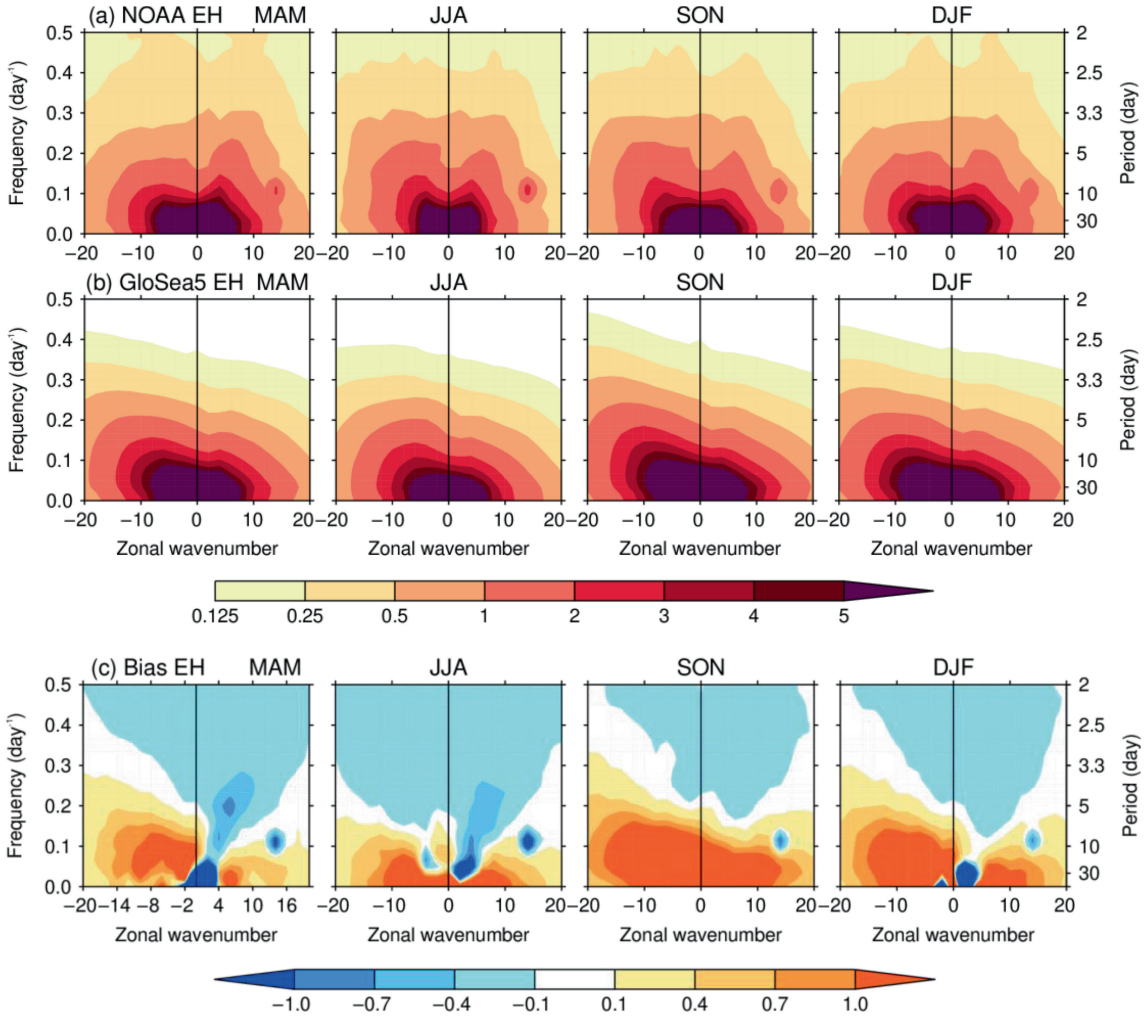

FIGURE 8 Seasonal zonal wave-number–frequency raw power spectra of OLR averaged at 15°N–15°S in the EH for (a) NOAA, (b) GloSea5 and (c) bias of GloSea5.

earlier versions of Met Office UM (Yang *et al.*, 2009) and recent real-time global operational NWP forecasts (Yang *et al.*, 2021).

3.2 | ENSO-related variations

To examine the wave–ENSO relationship, El Niño and La Niña events are identified for each season using the NOAA Oceanic Niño Index (ONI). ONI is defined as the three-month running mean of the Extended Reconstruction SSTs Version 5 (ERSST.v5: Huang *et al.*, 2017) anomalies in the Niño 3.4 region (5°N–5°S, 120°–170°W).

Both the ONI and standardised ONI are considered when defining El Niño and La Niña events, as the standardised ONI is useful for seasons with small SST variability. An El Niño season is identified if ONI ≥ 1°C or standardised ONI ≥1 standard deviation that lasts for at least three consecutive months. A La Niña season is identified if ONI ≤ −1°C or standardised ONI ≤ −1 SD lasts for at least three consecutive months. The number of ENSO events varies with season, ranging from 2 to 5 for El Niño and 3 to 6 for La Niña in 1993–2015.

3.2.1 | ENSO variation in ambient zonal winds and convective activity

As both tropical ambient zonal winds and convective activity have large ENSO-related variability, they provide a background to understand the ENSO–wave relationship (e.g. Yang *et al.*, 2013, 2016). We first examine the ENSO-related variation in these two variables.

The analysis of the tropical ambient zonal winds in El Niño and La Niña events indicates that the observed wind pattern in La Niña events is quite similar to that in the climate mean but with a stronger amplitude. Figure 10 shows the ENSO-related variation of the equatorial (15°N–15°S) zonal winds (ΔU, El Niño minus La Niña) for both levels.

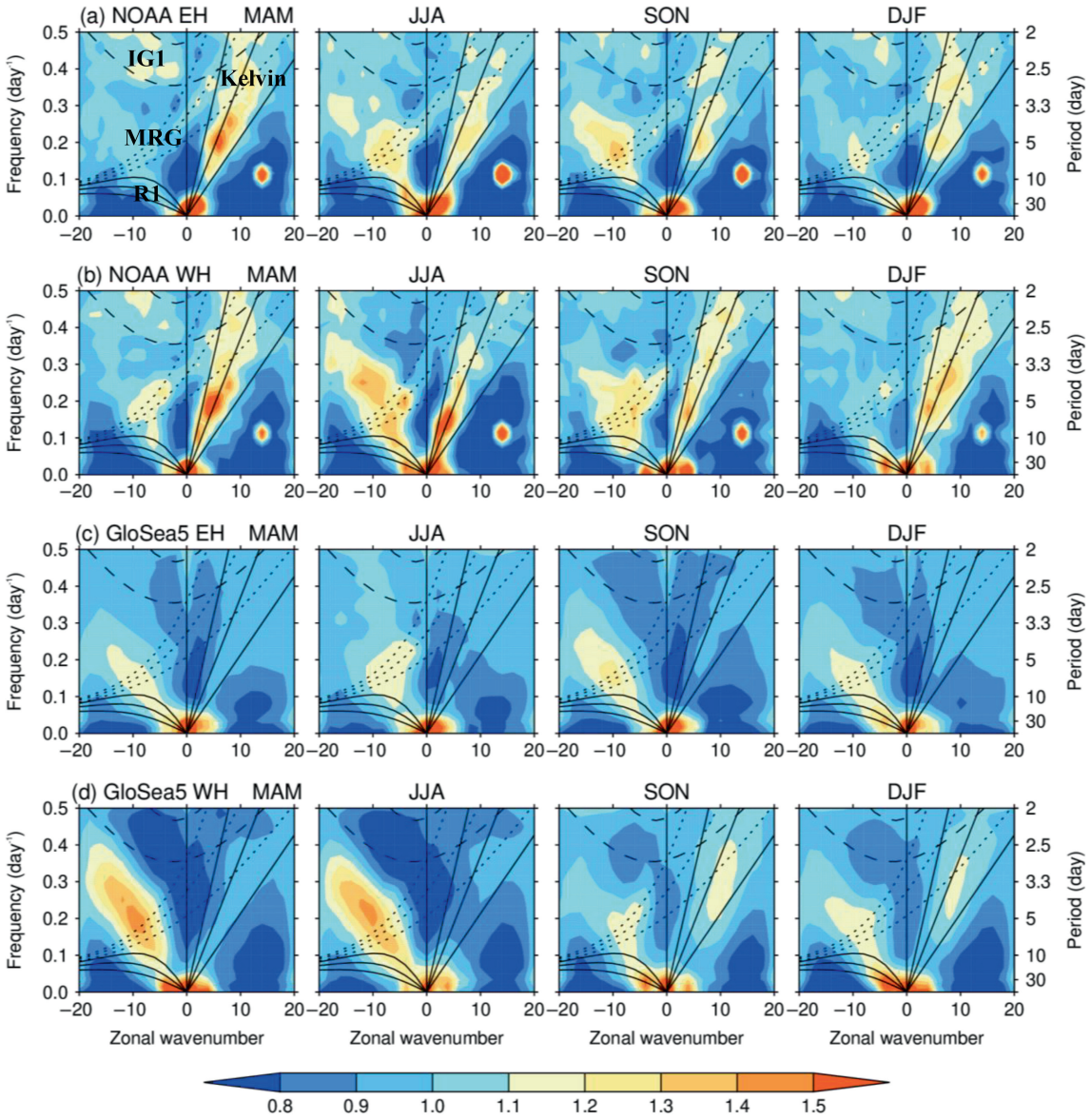

FIGURE 9 Seasonal zonal wave-number–frequency power spectra divided by background power for NOAA OLR in (a) EH, (b) WH, and for GloSea5 OLR in (c) EH and (d) WH. The power has been averaged over 15°N–15°S. Superimposed lines are the dispersion curves for the Kelvin wave (solid for $k > 0$), $n = 0$ MRG (dotted) and $n = 1$ R1 (solid for $k < 0$), and $n = 1$ inertial gravity waves (dashed) at the equivalent depths of 10, 30 and 90 m.

The upper-level winds in El Niño and La Niña events are shown in Figure S4. In the upper troposphere (Figure 10a and Figure S4), in ERA5, compared to La Niña events, the zonal wind pattern in El Niño events shows three distinct features. Firstly, the easterly wind in the Indian Ocean is weaker and shifts eastwards. Secondly, the westerly duct over the eastern Pacific is much weaker whereas the westerly duct over the Atlantic is slightly stronger, especially in the extended boreal winter, consistent with that found in ERA-Interim (Yang and Hoskins, 2013, 2016). Thirdly, from JJA to SON, the easterly flow between the eastern Pacific and Atlantic, which exists in the climatology (Figure 1) and La Niña (Figure S4), is replaced by westerly flow. The lower-tropospheric winds have opposite ENSO-related variation (Figure 10b). These changes are associated with a weaker Walker circulation in El Niño than in La Niña events.

GloSea5 can reproduce the observed ENSO-related zonal wind variation, but the upper-level variation shows a weaker amplitude in the Indo-Pacific region. Again, as in the climatology, the Atlantic westerly bias appears in both ENSO phases (Figure S4), especially in boreal summer and autumn.

To measure the forecast performance, the dotted regions in Figure 10c (right column) show the interannual correlations (significant at the 95% confidence level)

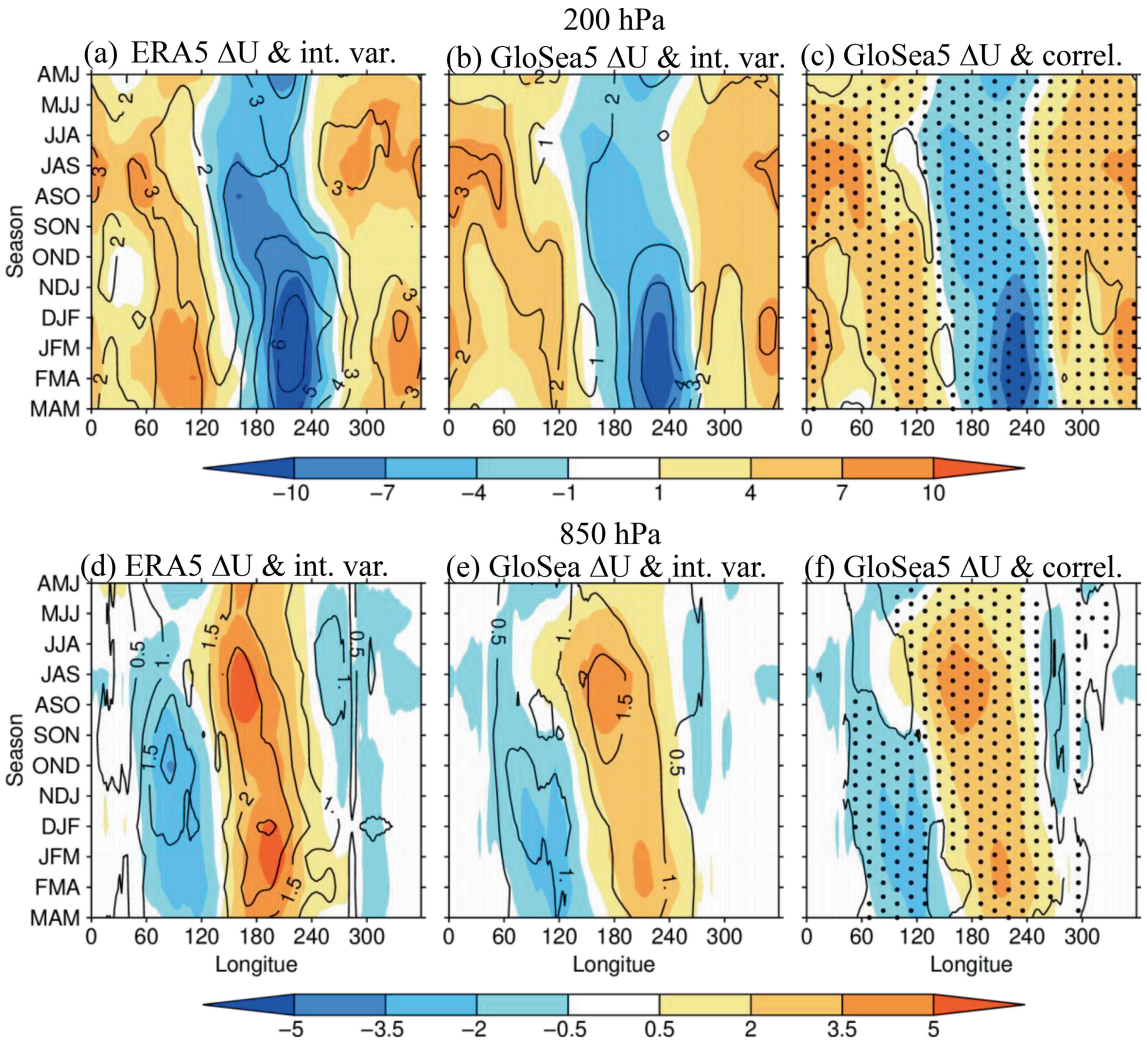

FIGURE 10 ENSO variation (El Niño − La Niña, colours) of equatorial (15°N–15°S) basic zonal wind (ΔU) in ERA5 and GloSea5, at (a–c) 200 hPa and (d–f) 850 hPa. Black contours in the left and middle columns show the interannual variability of U with a contour interval of 1 m·s^{-1} for 200 hPa and 0.5 m·s^{-1} at 850 hPa. The dotted areas in the right column indicate correlations between observed and GloSea5 U significant at the 95% confidence level, note in this column ΔU is shown again.

between the seasonal mean zonal winds of ERA5 and GloSea5. A significant correlation appears in most seasons and regions, indicating a good consistency between the interannual variability of zonal winds in ERA5 and GloSea5. The superimposed black contours in the left and middle columns of Figure 10 show the interannual variability in ERA5 and GloSea5, respectively. In both of them, the regions with larger ENSO variation are those regions with larger interannual variability, indicating that ENSO is the dominant mode in the interannual variability of the zonal winds.

The ENSO-related variations in the near-equatorial (15°N–15°S) OLR SDs for eastward and westward components are shown in Figure 11a,b, respectively. A distinct feature in observations is that in El Niño events the tropical convection is enhanced over the central-eastern Pacific but suppressed over the Indian to western Pacific region. This relationship between the ENSO phase and convection is well simulated in GloSea5, as indicated by the significant correlations over a wide area of the Indo-Pacific region (dotted regions in the third column in Figure 11).

Figures 12 and 13 show the OLR power spectra for El Niño and La Niña in the EH and WH, respectively. The observed wave-related convective signal varies with the ENSO phase and hemisphere. In the EH (Figure 12), the observed wave-related convective signal (Figure 12a,b) is weaker in El Niño than in La Niña events, for both the Kelvin wave (except in MAM) and the westward-moving MRG wave.

However, in GloSea5 (Figure 12c,d) there is no Kelvin wave-related convection in the EH for both ENSO phases. In contrast, GloSea5 catches the observed ENSO-related variation in the MRG-wave related convection except in

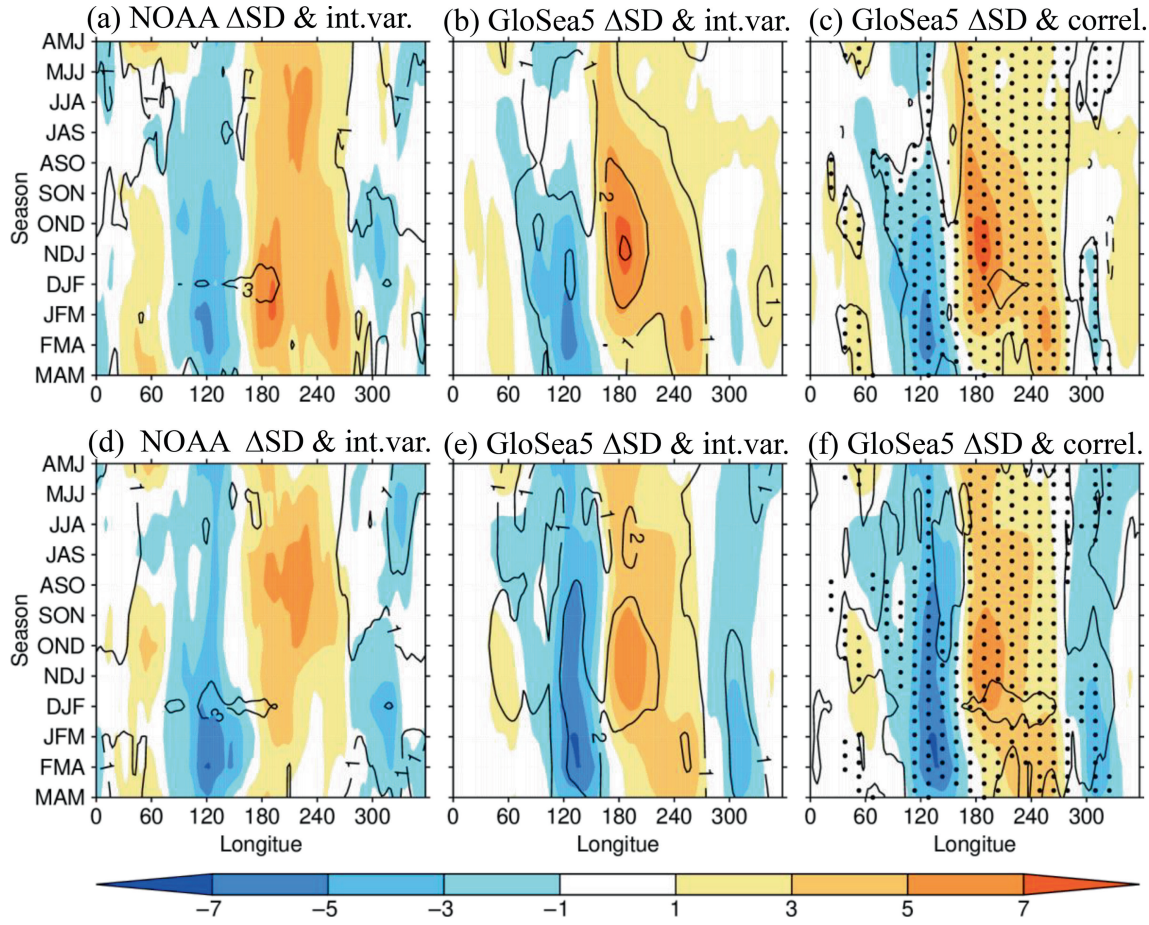

FIGURE 11 ENSO variation (El Niño − La Niña; colours) of equatorial (15°N–15°S) OLR SD (ΔSD) for (a–c) eastward-moving component and (d–f) westward-moving component, in NOAA and GloSea5. Black contours in the left and middle columns show the interannual variability of OLR SD with a contour interval of 2 $W \cdot m^{-2}$. The dotted areas in the right column indicate correlations between observed and GloSea5 OLR SD significant at the 95% confidence level.

MAM. In GloSea5, the R1-relative convective signal also exhibits a similar ENSO variation to that seen for the MRG, whereas in observations, the R1 wave ENSO variation is not clear.

In the WH (Figure 13), the observed Kelvin wave-related convection (Figure 13a,b) shows a dominant ENSO-variation in all seasons, being much stronger in El Niño than in La Niña, opposite to that in the EH. On the other hand, for the observed westward-moving convection, its relationship with ENSO varies with season. In JJA and SON, the power is stronger in El Niño than in La Niña, whereas the change reverses in MAM and is not clear in DJF. GloSea5 to some extent can reproduce the ENSO variation of Kelvin wave-related convection in SON and DJF in the WH (Figure 13c,d); however, the amplitudes are much weaker. In MAM and JJA, the model fails to simulate the Kelvin wave-related convection in both ENSO phases. This deficiency is consistent with the too weak Kelvin wave winds in GloSea5. On the other hand, GloSea5 does not have a clear ENSO-related variation in the westward-moving convection, and it has more power spreading to higher frequency and larger wave-number band which is related to tropical depressions.

3.2.2 | ENSO-related variation in the Kelvin wave

Figure 14 shows the ENSO-related variation (El Niño minus La Niña) in the Kelvin wave activity. The variation in ERA5 shows a complex pattern at 200 hPa (Figure 14a) due to the compound effects of the tropical ambient zonal flow, extratropical forcing and convective activity, and the relative importance of these effects varying with seasons. In the EH, the observed ENSO-related variation of Kelvin waves shows a positive variation in 120–180°E in the extended boreal summer, consistent with the easterly anomaly (Figure 10a) there, due to the fact that in El Niño the easterly wind in the Indian Ocean is weaker and shifts eastwards (Figure S4). In the extended boreal

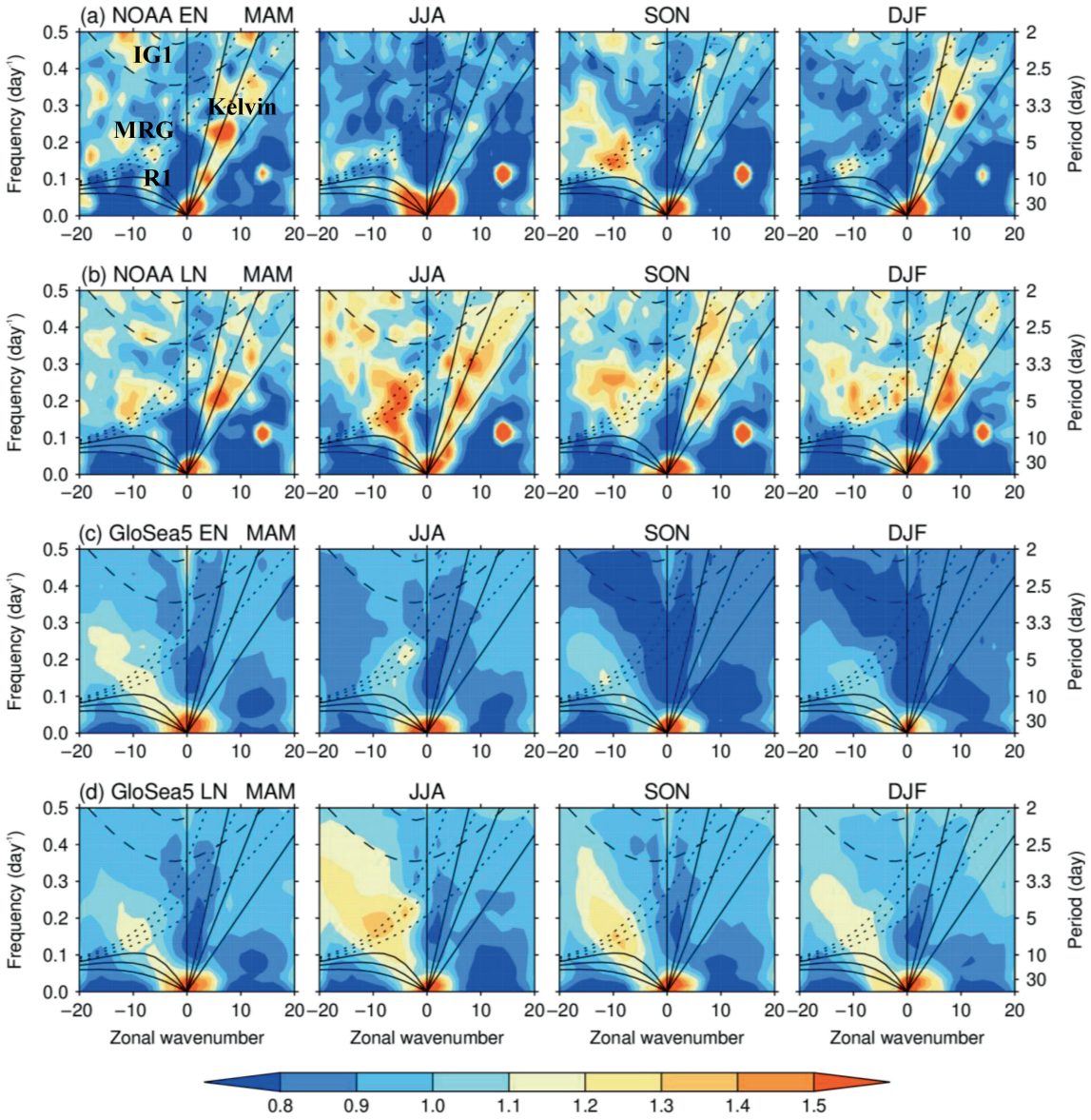

FIGURE 12 Seasonal zonal wave-number–frequency power spectra of OLR divided by background power in the EH for (a) NOAA in El Niño, (b) NOAA in La Niña; (c) GloSea5 in El Niño, and (d) GloSea5 in La Niña. The remaining conventions are the same as in Figure 9.

winter, a positive variation occurs over the east Indian Ocean to the west Pacific. This is likely to be related to the fact that in El Niño winter the NH subtropical jet is stronger and shifted southwards, leading to stronger subtropical eastward-moving forcing in the Indian Ocean to west Pacific which laterally forces the Kelvin wave activity (Hoskins and Yang, 2000; Yang and Hoskins, 2016). In the eastern Pacific in boreal summer, when the westerly duct is weaker and hence the extratropical forcing is weak, the ENSO-related variation in convective activity plays a main role in the wave activity: enhanced convection in El Niño leads to a positive wave variation. For the negative variation around 240°E in July–September (JAS), this can be explained by the disappearance of easterly winds in the region in an El Niño event (Figure S4). In boreal winter, when the eastern Pacific westerly duct is stronger and hence the extratropical forcing is dominant, the stronger westerly duct in La Niña winter allows more NH extratropical Rossby wave activity to propagate equatorward and force Kelvin waves, so the ENSO variation is negative there. Over the boreal winter Atlantic region, the intensity of the westerly duct does not show a clear connection to the Kelvin wave activity, consistent with that found in Yang and Hoskins (2013). In boreal summer the Atlantic shows a positive variation there; the reason for this is not clear.

For GloSea5, the ENSO variation of Kelvin waves in the upper troposphere (Figure 14b) is more confined to the Pacific and Atlantic. GloSea5 to some extent can capture the observed variation in the central to eastern Pacific

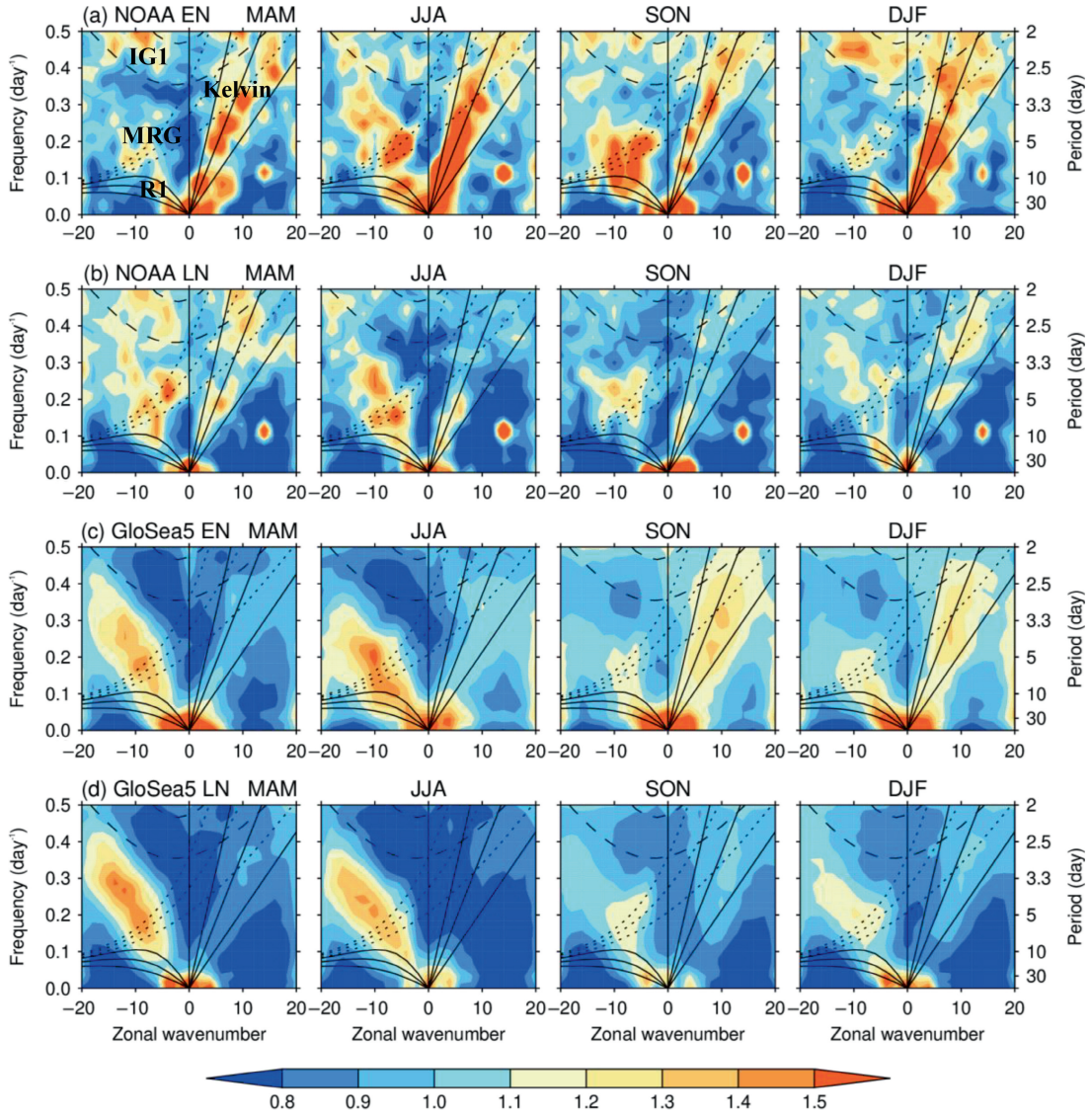

FIGURE 13 (a–d) As in Figure 12 but for WH zonal wave-number–frequency power spectra divided by background power.

but with a too weak amplitude, whereas in the Atlantic in the extended boreal winter GloSea5 presents an unrealistic strong positive variation there.

For the observed Kelvin wave activity at 850 hPa (Figure 14d), as the extratropical forcing is weak in the lower troposphere, the Kelvin wave ENSO variation is mainly connected to the variation of tropical convection, with the wave activity over the eastern Pacific being stronger in El Niño than La Niña, consistent with the stronger eastward-moving convective activity in El Niño (Figures 11 and 13). GloSea5 (Figure 14e) can capture the observed variation, but the positive variation in the eastern Pacific is again too weak, consistent with the generally too weak Kelvin wave winds (Figure 2) and wave-related convective signal in GloSea5 (Figure 13).

In both ERA5 and GloSea5, the regions with larger ENSO-variation of Kelvin waves are those with larger interannual variability (black solid lines in the left two columns in Figure 14), indicating that the interannual variability of Kelvin wave activity is dominated by ENSO. Significant correlations between ERA5 and GloSea5 (dotted areas in right panel of Figure 14) are concurrent with regions where the GloSea5 ENSO-variation is consistent with that of ERA5. This suggests that the forecast performance for wave activity is driven by the representation of the ENSO–wave teleconnection.

3.2.3 | ENSO-related variation in MRG waves

Figure 15 shows the ENSO-related variation of MRG waves. At 200 hPa, the observed ENSO variation of the MRG (Figure 15a) is dominated by a strong negative anomaly in the central-eastern Pacific in all seasons,

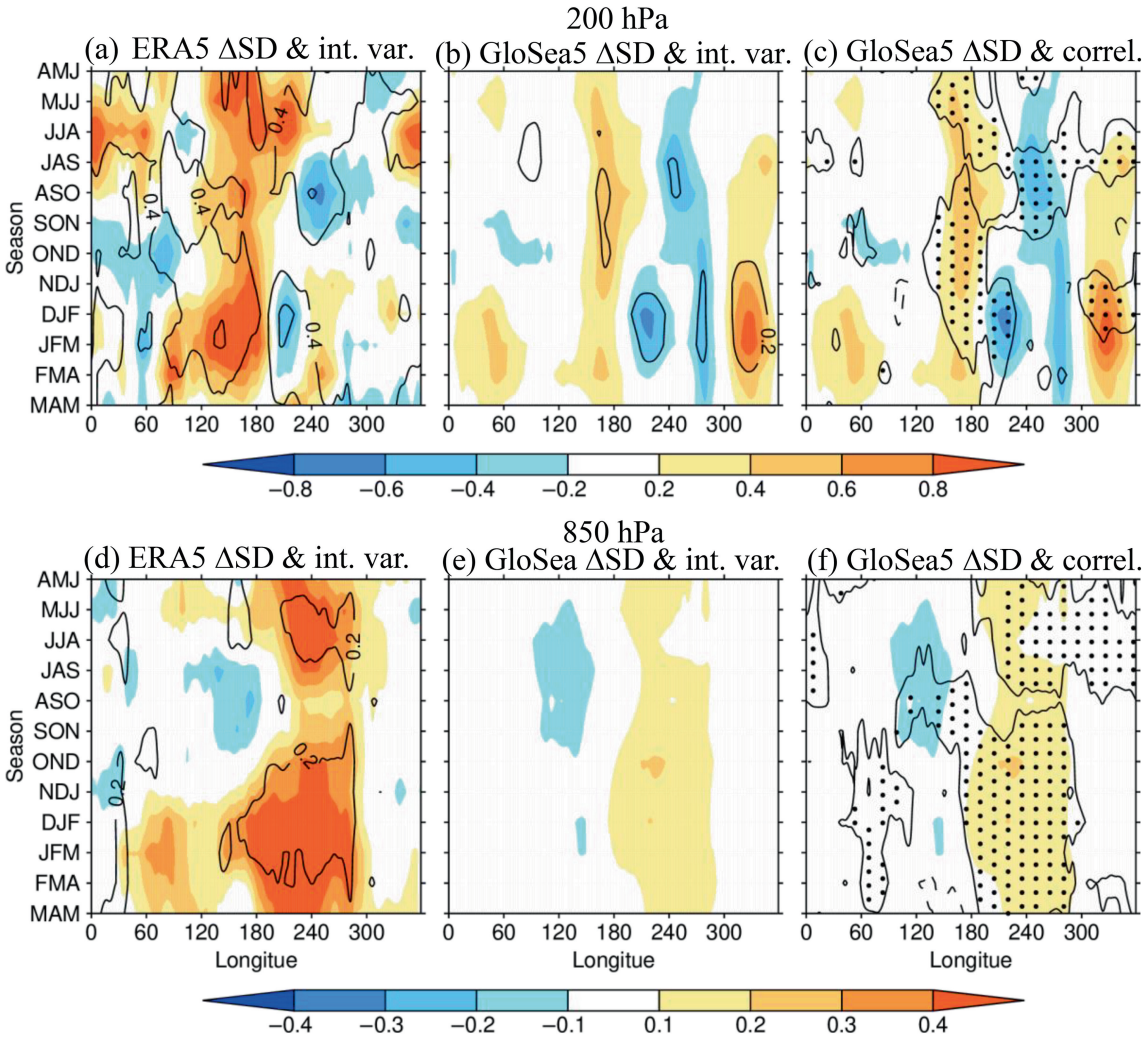

FIGURE 14 ENSO variation (El Niño minus La Niña: colours) of Kelvin wave activity in ERA5 and GloSea5, at (a–c) 200 hPa and (d–f) 850 hPa. Black contours in the left and middle columns show the interannual variability of Kelvin wave activity in ERA5 and the GloSea5 ensemble mean, respectively, with a contour interval of 0.2 $m \cdot s^{-1}$ at 200 hPa and 0.1 $m \cdot s^{-1}$ at 850 hPa, the same intervals as for the colours. The dotted areas in the third column indicate correlations between ERA5 and GloSea5 wave activity significant at the 95% confidence level, note in this column ΔSD is shown again.

especially in the extended boreal winter. A noticeable opposite-signed variation occurs in the Atlantic in DJF. The MRG–ENSO relationship is consistent with the ENSO-driven variation in the two westerly ducts (Figure 10a). There is also weak positive variation in the Indian to western Pacific, consistent with the westerly anomaly there (Figure 10a). GloSea5 is able to reproduce the observed upper-tropospheric MRG–ENSO variation in the Pacific, but in the Atlantic the ENSO-related positive variation is too weak in January–March (JFM) and February–April (FMA), and there is an unrealistic large region of strong negative variation in boreal summer (Figure 15b).

At 850 hPa, MRG–ENSO variation dominates in the Indo-Pacific (Figure 15d), with strong positive variation around 150–180°E in all seasons except JFM, and negative variation around 60–130°E for all seasons. The pattern of variation is well simulated by GloSea5 (Figure 15e). For both ERA5 and GloSea5, the ENSO-related MRG variation in the Indo-Pacific is consistent with their low-level ambient zonal flow variation (Figure 10d,e), with the westerly (easterly) anomaly corresponding to the positive (negative) variation of the MRG wave activity. The pattern of variation is also consistent with the ENSO-related variation in the westward-moving convective activity in most seasons (Figure 11d,e), with the positive (negative) variation in the convective activity appearing in the positive (negative) variation in the MRG wave activity.

The observed interannual variation in the wave activity is also well predicted by GloSea5 with a comparable magnitude. Again, significant correlations (Figure 15c,f)

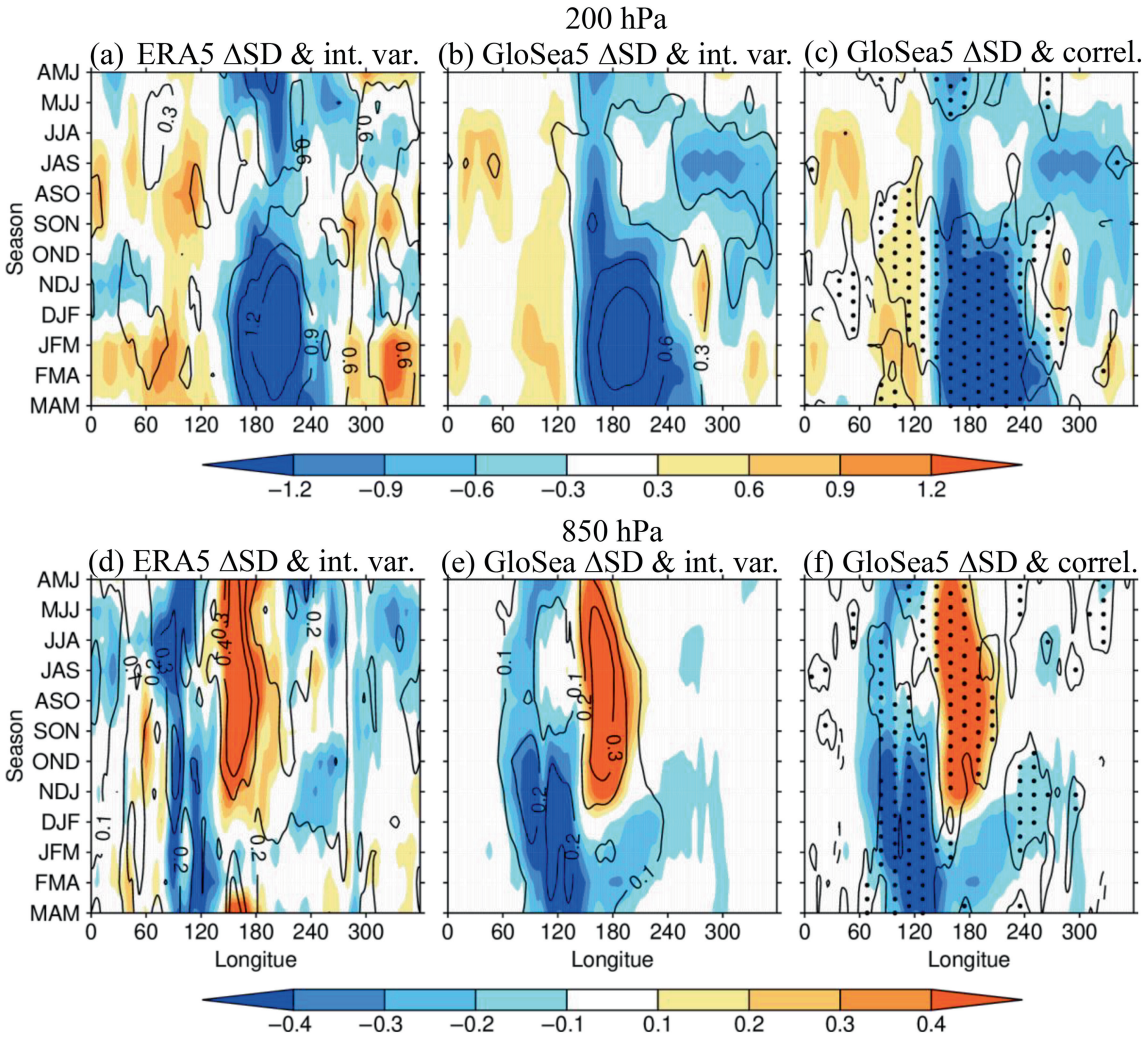

FIGURE 15 (a–f) As in Figure 14 but for MRG wave v on the Equator, and at 200 hPa (top) the black contour interval is 0.3 $m \cdot s^{-1}$.

between ERA5 and GloSea5 wave activity appear in the regions where the GloSea5 ENSO variation is consistent with that in ERA5.

3.2.4 | ENSO-related variations in R1 and R2 waves

Figure 16 shows the ENSO variation of R1 activity. As for the MRG, the observed R1 at 200 hPa (Figure 16a) has a strong negative variation in the central-eastern Pacific in the extended boreal winter. From America to the Atlantic, there are also various negative variations, which is different from that of the MRG. GloSea5 (Figure 16b) is able to capture these observed features.

At 850 hPa, the observed ENSO variation of R1 (Figure 16d) is similar to that for the MRG, but its negative variation in the Indian Ocean is weaker than that of the MRG in the extended boreal summer. GloSea5 (Figure 16e) reproduces the observed variation reasonably well. The interannual variability of the R1 in GloSea5 is comparable to that in ERA5. As in the Kelvin wave and MRG wave, significant correlations of wave activity between ERA5 and GloSea5 are concurrent with regions where the GloSea5 ENSO-variation is consistent with that of ERA5, indicating that the ENSO–wave teleconnections are well represented in the model.

The results for R2 are shown in Figure S5. The observed upper-level R2 variation (Figure S5a) indicates a strong negative variation in the eastern Pacific in the extended boreal winter, similar to that of the MRG and R1. GloSea5 (Figure S5b) can capture the negative variation. The observed low-level R2 variation (Figure S5d) indicates a similar positive variation in the western Pacific in the extended boreal summer as for the MRG and R1, but the negative variation in the Indian Ocean is less clear. GloSea5 can reproduce the positive variation in the western Pacific, but presents an unrealistic strong negative variation over the central Pacific in the extended boreal winter.

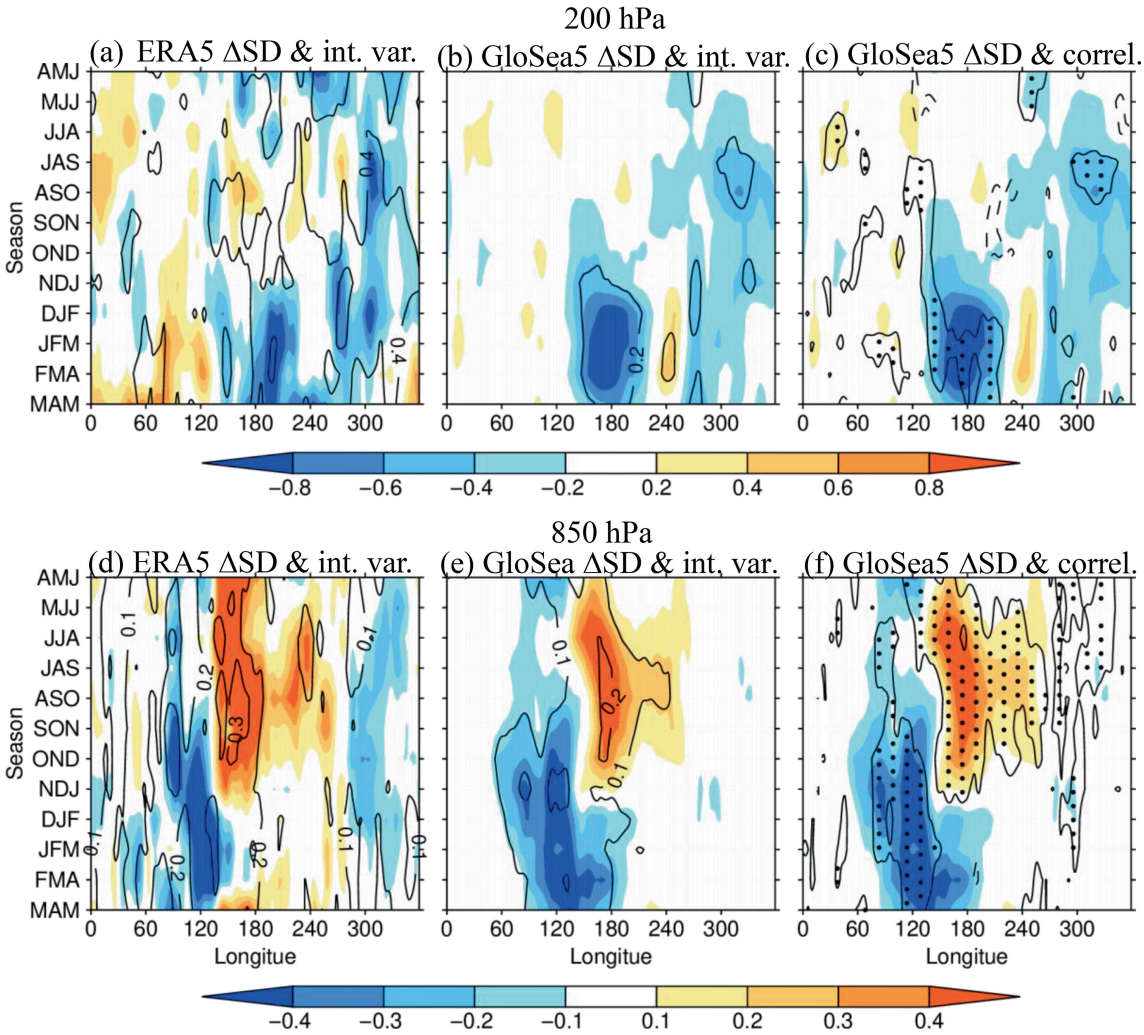

FIGURE 16 (a–f) As in Figure 14 but for R1 wave v at 8°N.

4 | SUMMARY AND DISCUSSION

The method of spatial projection based on equatorial wave theory is used in this article to identify equatorial waves in ERA5 and GloSea5. The seasonal variation, longitudinal distribution and interannual variability of equatorial wave activity, including the ENSO–wave teleconnections, are investigated. The extent to which GloSea5 is able to represent the observed wave behaviour and their relationship with ENSO is examined. The tropical ambient zonal flow and tropical convection are also investigated to interpret the behaviour of the equatorial wave activity in ERA5 and the GloSea5 seasonal forecasts.

The results showed that the seasonal and longitudinal distribution of equatorial wave activity is largely determined by the tropical mean ambient zonal flow, the associated upper-tropospheric extratropical forcing and tropical convective activity. The Kelvin wave activity in ERA5 is mainly determined by the ambient flow in both the upper and lower troposphere, with the maximum wave activity appearing in the easterly regions of the Indian Ocean–western Pacific in the upper troposphere and eastern Pacific in the lower troposphere, as suggested by the impact mechanisms discussed in Section 2.3. The westward-moving MRG, R1 and R2 waves in the upper troposphere are closely connected to the ambient zonal flow in the EH and extratropical forcing in the WH, with stronger wave activity appearing in the ambient westerly flow. The westward-moving waves in the lower troposphere are connected to the ambient flow and tropical convective activity.

For the Kelvin wave, GloSea5 does not well simulate the seasonal and longitudinal pattern in the upper troposphere, and underestimates the wave activity in both the upper and lower troposphere. This is consistent with the fact that GloSea5 has too weak eastward-moving convective activity near the equatorial region and the signal related to Kelvin waves is entirely missing in the climate mean.

On the other hand, GloSea5 performs better for the westward-moving MRG, R1 and R2 waves in both the upper and lower troposphere, including their Doppler-shifted eastward-moving components in the WH upper troposphere. GloSea5 can capture the seasonal and longitudinal distribution of these wave activities, in particular the strong upper-level wave activity over the eastern Pacific owing to the good simulation of the westerly duct there, and the strong low-level activity in oceanic regions. However, there are biases in the magnitude. GloSea5 overestimates the upper-level wave activities in the WH, especially for MRG waves, due to a systematic westerly bias in the Atlantic. GloSea5 also overestimates the low-level wave activity in the western Pacific for all three westward-moving waves in all seasons, but underestimates the wave activity in the Indian Ocean in the extended boreal summer for the MRG and R1. The bias pattern in the Indo-Pacific resembles the biases of the low-level ambient flow, with too strong wave activity coincident with the westerly bias and too weak wave activity coincident with the easterly bias. The wave bias also relates to the bias of the westward-moving convective activity, with too strong wave activity in the western Pacific coincident to the too strong westward-moving convective activity there. The generally too strong low-level wave bias in the western Pacific may be responsible for the excessive tropical cyclone activity in the region in GloSea5 (Feng *et al.*, 2020), since the westward-moving equatorial waves can significantly impact tropical cyclones (Feng *et al.*, 2023).

The finding that GloSea5 has relatively poor performance in simulating the Kelvin waves but performs better in simulating the westward-moving equatorial waves is consistent with that found in the older versions of the Met Office Unified Model (UM) (Yang *et al.*, 2009), suggesting a systematic bias in the model. Also, consistent with Yang *et al.* (2009), the poor performance of GloSea5 in simulating Kelvin waves seems to be associated with its deficiency in simulating near-equatorial eastward-moving convection which is often coupled with Kelvin waves.

For the interannual variability of the waves, GloSea5 does not predict well the ENSO-variation of Kelvin waves in the upper troposphere, due to the fact that the upper-level Kelvin waves are impacted not only by the ENSO-driven variation in the ambient zonal flow, but also by the ENSO-variation in the extratropical forcing, which could be misrepresented in GloSea5. On the other hand, GloSea5 can capture the Kelvin wave–ENSO relationship in the lower troposphere reasonably well over the eastern Pacific, with stronger wave activity over the eastern Pacific in El Niño, due to the good performance for the ENSO-related variation in tropical convection, although the magnitude of the ENSO variation in the Kelvin wave is too weak.

For the westward-moving equatorial waves, GloSea5 predicts well the ENSO–wave relationship, except for the MRG wave in the upper-tropospheric Atlantic due to the strong westerly biases there. In the upper troposphere, the ERA5 westward-moving wave activity over the eastern Pacific is consistently weaker in El Niño than in La Niña, which is well represented by GloSea5 due to its good performance in simulating the ENSO-driven variation in the intensity of the westerly duct there. In the lower troposphere, GloSea5 also well captures the observed feature that the wave activity is stronger over the western to central Pacific but weaker in the Indian Ocean to western Pacific in El Niño, owing to the fact that GloSea5 can capture the ENSO-variation in the low-level ambient zonal flow and westward-moving tropical convective activity.

For the interannual variability of the waves, the regions and seasons with the best forecast performance are coincident and collocated with regions and seasons in which the wave–ENSO relationship is well simulated in GloSea5. This suggests that the interannual variability of GloSea5 wave activity is dominated by ENSO, and correctly representing the ENSO–wave teleconnection in GloSea5 is key to seasonal forecasting of wave activity.

The poor performance of GloSea5 in simulating the ENSO–Kelvin wave teleconnection is consistent with the model deficiency in simulating the convective signal connected to the Kelvin waves. The better performance of GloSea5 in simulating the ENSO-variation in the westward-moving equatorial waves seems to be attributed to its good simulation of the ENSO-driven variation in the tropical ambient flow and the associated extratropical forcing, and the westward-moving tropical convective activity.

The biases in GloSea5, such as the too strong convective power at low frequencies, too weak Kelvin wave activity and associated convection, are worthy of further investigation, since too much convective variance at lower frequencies would lead to too persistent tropical precipitation, and correctly simulating the convectively coupled Kelvin waves would provide an important resource in predicting tropical extreme precipitation (Ferrett *et al.*, 2020, 2023). For future work, it would be interesting to explore the detailed coupling of equatorial waves with convection in both reanalyses and models.

AUTHOR CONTRIBUTIONS

Gui-Ying Yang: Conceptualization; data curation; formal analysis; investigation; methodology; software; visualization; writing – original draft. **Xiangbo Feng:** Conceptualization; project administration; writing – review and editing. **Kevin Hodges:** Conceptualization; data curation; writing – review and editing.

ACKNOWLEDGEMENTS

This work and its contributors were supported by the Weather and Climate Science for Services Partnership (WCSSP) Southeast Asia as part of the Newton Fund. Gui-Ying Yang was also supported by the National Centre for Atmospheric Science through the NERC National Capability International Programmes Award (NE/X006263/1). We would like to thank Dr Nick Klingaman for his contribution and useful comments in the early stages of the project leading to this article.

DATA AVAILABILITY STATEMENT

GloSea5 reforecast data are archived through the sub-seasonal to seasonal prediction (S2S) project (https://confluence.ecmwf.int/display/S2S/S2S+archive). The ERA5 data (Hersbach *et al.*, 2020) is generated by ECMWF and distributed by the Climate Data Store (CDS), under the Copernicus Climate Change Service (C3S). The OLR data (Liebmann and Smith, 1996) are available at https://psl.noaa.gov/data/gridded/data.interp_OLR.html. Computing and data storage facilities were provided by JASMIN (https://jasmin.ac.uk).

ORCID

Gui-Ying Yang https://orcid.org/0000-0001-7450-3477
Xiangbo Feng https://orcid.org/0000-0003-4143-107X

REFERENCES

Ayesiga, G., Holloway, C.E., Williams, C.J.R., Yang, G.-Y., Stratton, R. and Roberts, M. (2022) Linking equatorial African precipitation to kelvin wave processes in the CP4-Africa convection-permitting regional climate simulation. *Journal of the Atmospheric Sciences*, 79, 1271–1289.

Baldwin, M.P., Gray, L.J., Dunkerton, T.J., Hamilton, K., Haynes, P.H., Randel, W.J., Holton, J.R., Alexander, M.J., Hirota, I., Horinouchi, T., Jones, D.B.A., Kinnersley, J.S., Marquardt, C., Sato, K. and Takahashi, M. (2001) The quasi-biennial oscillation. *Reviews of Geophysics*, 39, 179–229.

Charney, J.G. (1969) A further note on large-scale motions in the tropics. *Journal of the Atmospheric Sciences*, 26, 182–185.

Cheng, Y.-M., Tulich, S., Kiladis, G.N. and Dias, J. (2022) Two extratropical pathways to forcing tropical convective disturbances. *Journal of Climate*, 35, 2987–3009.

Dias, J. and Kiladis, G.N. (2014) Influence of the basic state zonal flow on convectively coupled equatorial waves. *Geophysical Research Letters*, 41, 6904–6913.

Feng, X., Klingaman, N.P., Hodges, K.I. and Guo, Y.P. (2020) Western North Pacific tropical cyclones in the Met Office global seasonal forecast system: performance and ENSO teleconnections. *Journal of Climate*, 33, 10489–10504.

Feng, X., Yang, G.-Y., Hodges, K.I. and Methven, J. (2023) Equatorial waves as useful precursors to tropical cyclone occurrence and intensification. *Nature Communications*, 14(1), 511.

Ferrett, S.J., Methven, J., Woolnough, S.J., Yang, G.-Y. and Holloway, C.E. (2023) Hybrid dynamical-statistical forecasts of the risk of rainfall in South East Asia conditional on equatorial waves. *Monthly Weather Review*. https://doi.org/10.1175/MWR-D22-0300.1

Ferrett, S.J., Yang, G.-Y., Woolnough, S.J., Methven, J., Hodges, K. and Holloway, C.E. (2020) Linking extreme precipitation in Southeast Asia to equatorial waves. *Quarterly Journal of the Royal Meteorological Society*, 146, 665–684.

Gehne, M. and Kleeman, R. (2012) Spectral analysis of tropical atmospheric dynamical variables using a linear shallow-water modal decomposition. *Journal of the Atmospheric Sciences*, 69, 2300–2316.

Gill, A.E. (1980) Some simple solutions for heat induced tropical circulations. *Quarterly Journal of the Royal Meteorological Society*, 106, 447–462.

Hayashi, Y. (1982) Space-time spectral analysis and its applications to atmospheric waves. *Journal of the Meteorological Society of Japan*, 60, 156–171. https://doi.org/10.2151/jmsj1965.60.1_156.

Hersbach, H., Bell, B., Berrisford, P., Hirahara, S., Horányi, A., Muñoz-Sabater, J., Nicolas, J., Peubey, C., Radu, R., Schepers, D. and Simmons, A. (2020) The ERA5 global reanalysis. *Quarterly Journal of the Royal Meteorological Society*, 146, 1999–2049.

Hoskins, B.J., Yang, G.-Y. and Fonseca, R.M. (2020) The detailed dynamics of the June-August Hadley cell. *Quarterly Journal of the Royal Meteorological Society*, 146, 557–575.

Hoskins, B.J. and Yang, G.-Y. (2000) The equatorial response to high-latitude forcing. *Journal of the Atmospheric Sciences*, 57, 1197–1213.

Hoskins, B.J. and Yang, G.-Y. (2016) The longitudinal variation of equatorial waves due to propagation on a zonal varying flow. *Journal of the Atmospheric Sciences*, 73, 605–620.

Hoskins, B.J. and Yang, G.-Y. (2021) The detailed dynamics of the Hadley cell. Part II: December-February. *Journal of Climate*, 34, 805–823.

Huang, B., Thorne, P.W., et al. (2017) Extended Reconstructed Sea surface temperature version 5 (ERSSTv5), upgrades, validations, and intercomparisons. *Journal of Climate*, 30, 8179–8205. https://doi.org/10.1175/JCLI-D-16-0836.1.

Hung, M.-P., Lin, J.-L., Wang, W., Kim, D., Shinoda, T. and Weaver, S.J. (2013) MJO and convectively coupled equatorial waves simulated by CMIP5 climate models. *Journal of Climate*, 26, 6185–6214.

Judt, F. (2020) Atmospheric predictability of the tropics, middle latitudes, and polar regions explored through global storm resolving simulations. *Journal of the Atmospheric Sciences*, 77, 257–276.

Kiladis, G.N. (1998) Observations of Rossby waves linked to convection over the eastern tropical Pacific. *Journal of the Atmospheric Sciences*, 55, 321–339.

Kiladis, G.N., Dias, J. and Gehne, M. (2016) The relationship between equatorial mixed Rossby-gravity and eastward inertio-gravity waves. Part I. *Journal of the Atmospheric Sciences*, 73, 2123–2145.

Kiladis, G.N., Wheeler, M.C., Haertel, P.T., Straub, K.H. and Roundy, P.E. (2009) Convectively coupled equatorial waves. *Reviews of Geophysics*, 47, RG2003.

Knippertz, P., Gehne, M., Kiladis, G.N., Kikuchi, K., Satheesh, A.R., Roundy, P.E., Yang, G.-Y., Žagar, N., Dias, J., Fink, A.H., Methven, J., et al. (2022) The intricacies of identifying equatorial waves. *Quarterly Journal of the Royal Meteorological Society*, 148, 2814–2852.

Lau, K.-M. (1981) Oscillations in a simple equatorial climate system. *Journal of the Atmospheric Sciences*, 38, 248–261.

Lau, K.-M. and Peng, L. (1987) Origin of low frequency (intraseasonal) oscillations in the tropical atmosphere. Part I: basic theory. *Journal of the Atmospheric Sciences*, 44, 950–972.

Li, Y. and Stechmann, S.N. (2020) Predictability of tropical rainfall and waves: estimates from observational data. *Quarterly Journal of the Royal Meteorological Society*, 146, 1668–1684. https://doi.org/10.1002/qj.3759.

Liebmann, B. and Smith, C.A. (1996) Description of a complete (interpolated) outgoing longwave radiation dataset. *Bulletin of the American Meteorological Society*, 77, 1275–1277.

Lim, H. and Chang, C.-P. (1983) Dynamics of teleconnections and Walker circulations forced by equatorial heating. *Journal of the Atmospheric Sciences*, 40, 1897–1915.

Lin, J.-L., Weickmann, K.M., Sperber, K.R., Lin, W., Wheeler, M.C., Schubert, S.D. and Del Genio, A. (2006) Tropical intraseasonal variability in 14 IPCC AR4 climate models. Part I: convective signals. *Journal of Climate*, 19, 2665–2690.

Lindzen, R.S. and Holton, J.R. (1968) A theory of the quasi-biennial oscillation. *Journal of the Atmospheric Sciences*, 25, 1095–1107.

Magaña, V. and Yanai, M. (1995) Mixed Rossby–gravity waves triggered by lateral forcing. *Journal of the Atmospheric Sciences*, 52, 1473–1486.

Masunaga, H. (2007) Seasonality and regionality of the Madden-Julian oscillation, kelvin wave, and equatorial Rossby wave. *Journal of the Atmospheric Sciences*, 64, 4400–4416.

Pahlavan, H.A., Wallace, J.M., Fu, Q. and Kiladis, G.N. (2021) Revisiting the quasi-biennial oscillation as seen in ERA5. Part II: evaluation of waves and wave forcing. *Journal of the Atmospheric Sciences*, 78, 693–707.

Peatman, S.C., Schwendike, J., Birch, C.E., Marsham, J.H., Matthews, A.J. and Yang, G.-Y. (2021) A local-to-large scale view of Maritime Continent rainfall: control by ENSO, MJO, and equatorial waves. *Journal of Climate*, 34(22), 8933–8953.

Ringer, M.A., Martin, G.M., Greeves, C.Z., Hinton, T.J., James, P.M. and Pope, V. (2006) The physical properties of the atmosphere in the New Hadley Centre Global Environmental Model (HadGEM1). Part II: aspects of variability and regional climate. *Journal of Climate*, 19, 1302–1326.

Roundy, P.E. (2008) Analysis of convectively coupled kelvin waves in the Indian Ocean MJO. *Journal of the Atmospheric Sciences*, 65, 1342–1359.

Straub, K.H. and Kiladis, G.N. (2003) Extratropical forcing of convectively coupled kelvin waves during austral winter. *Journal of the Atmospheric Sciences*, 60, 526–543.

Takayabu, Y.N. (1994) Large-scale cloud disturbances associated with equatorial waves. Part I: spectral features of the cloud disturbances. *Journal of the Meteorological Society of Japan*, 72, 433–448.

Tomassini, L. and Yang, G.-Y. (2022) Tropical moist convection as an important driver of Atlantic Hadley circulation variability. *Quarterly Journal of the Royal Meteorological Society*, 148, 3287–3302.

Tulich, S.N. and Kiladis, G.N. (2021) On the regionality of moist kelvin waves and the MJO: the critical role of the background zonal flow. *Journal of Advances in Modeling Earth Systems*, 13, e2021MS002528.

Wang, B. and Xie, X. (1996) Low-frequency equatorial waves in vertically sheared zonal flow. Part I: stable waves. *Journal of the Atmospheric Sciences*, 53, 449–467.

Webster, P.J. and Holton, J.R. (1982) Cross-equatorial response to mid-latitude forcing in a zonally varying basic state. *Journal of the Atmospheric Sciences*, 39, 722–733.

Wheeler, M. and Kiladis, G.N. (1999) Convectively coupled equatorial waves: analysis of clouds and temperature in the wavenumber-frequency domain. *Journal of the Atmospheric Sciences*, 56, 374–399.

Wheeler, M., Kiladis, G.N. and Webster, P. (2000) Large-scale dynamical fields associated with convectively coupled equatorial waves. *Journal of the Atmospheric Sciences*, 57, 613–640.

Wheeler, M.C., Zhu, H., Sobel, A.H., Hudson, D. and Vitart, F. (2017) Seamless precipitation prediction skill comparison between two global models. *Quarterly Journal of the Royal Meteorological Society*, 143, 374–383.

Yang, G.-Y., Ferrett, S., Woolnough, S., Methven, J. and Holloway, C. (2021) Real-time identification of equatorial waves and evaluation of waves in global forecasts. *Weather and Forecasting*, 36, 171–193.

Yang, G.-Y. and Hoskins, B.J. (1996) Propagation of Rossby wave of nonzero frequency. *Journal of the Atmospheric Sciences*, 53, 2365–2378.

Yang, G.-Y. and Hoskins, B.J. (2013) ENSO impact on kelvin waves and associated tropical convection. *Journal of the Atmospheric Sciences*, 70, 3513–3532.

Yang, G.-Y. and Hoskins, B.J. (2016) ENSO-related variation of equatorial MRG and Rossby waves and forcing from higher latitudes. *Quarterly Journal of the Royal Meteorological Society*, 142, 2488–2504.

Yang, G.-Y., Hoskins, B.J. and Gray, L. (2012) The influence of the QBO on the propagation of equatorial waves into the stratosphere. *Journal of the Atmospheric Sciences*, 69, 2959–2982.

Yang, G.-Y., Hoskins, B.J. and Slingo, J.M. (2003) Convectively coupled equatorial waves: a new methodology for identifying wave structures in observational data. *Journal of the Atmospheric Sciences*, 60, 1637–1654.

Yang, G.-Y., Hoskins, B.J. and Slingo, J.M. (2007a) Convectively coupled equatorial waves: part I: horizontal structure. *Journal of the Atmospheric Sciences*, 64, 3406–3423.

Yang, G.-Y., Hoskins, B.J. and Slingo, J.M. (2007b) Convectively coupled equatorial waves: part II: zonal propagation. *Journal of the Atmospheric Sciences*, 64, 3424–3437.

Yang, G.-Y., Hoskins, B.J. and Slingo, J.M. (2007c) Convectively coupled equatorial waves: part III: Synthesis structures and extratropical forcing. *Journal of the Atmospheric Sciences*, 64, 3438–3451.

Yang, G.-Y., Slingo, J. and Hoskins, B.J. (2011) Equatorial waves in opposite QBO phases. *Journal of the Atmospheric Sciences*, 68, 839–862.

Yang, G.-Y., Slingo, J.M. and Hoskins, B.J. (2009) Convectively coupled equatorial waves in high resolution Hadley centre climate models. *Journal of Climate*, 22, 1897–1919.

Yang, G.-Y., Methven, J., Woolnough, S.J., Hodges and Hoskins, B.J. (2018) Linking African Easterly Wave activity with equatorial waves and influence of Rossby waves from the Southern Hemisphere. *Journal of the Atmospheric Sciences*, 75, 1783–1809.

Yu, X. and McPhaden, M.J. (1999) Seasonal variability in the equatorial Pacific. *Journal of Physical Oceanography*, 29, 925–947.

Zhang, C. (1993) Laterally forced equatorial perturbations in linear model. Part II: mobile forcing. *Journal of the Atmospheric Sciences*, 50, 807–821.

SUPPORTING INFORMATION

Additional supporting information can be found online in the Supporting Information section at the end of this article.

How to cite this article: Yang, G.-Y., Feng, X. & Hodges, K. (2023) Seasonal and interannual variation of equatorial waves in ERA5 and GloSea5. *Quarterly Journal of the Royal Meteorological Society*, 1–26. Available from: https://doi.org/10.1002/qj.4460